Depletion of dAKAP1 signaling complexes accompanies pathological changes in mitochondrial dynamics during breast cancer progression.

Stacey Aggarwal

A dissertation

submitted in partial fulfillment of the

requirements for the degree of

Doctor of Philosophy

University of Washington

2018

Reading Committee:

John D. Scott, Chair

Yasemin Sancak

Shao-En Ong

Program authorized to offer degree:

Pharmacology

University of Washington

Abstract

Depletion of dAKAP1 signaling complexes accompanies pathological changes in mitochondrial dynamics during breast cancer progression

Stacey Aggarwal

Chair of the Supervisory Committee:

John D. Scott

Department of Pharmacology

The dual-specificity A-kinase anchoring protein 1 (dAKAP1) is a mitochondrial anchoring protein responsible for recruiting protein kinase A (PKA), along with other signaling molecules, to the outer mitochondrial membrane to influence mitochondrial dynamics. Through careful analysis of publicly available proteomic and transcriptomic datasets, we have observed a marked inverse correlation of known mesenchymal markers with dAKAP1 expression in breast cancer cell lines and tissues. Furthermore, dAKAP1 expression also correlated with both oxidative metabolism and decreased motility in breast cancer cell lines. These data suggest that dAKAP1 may be down-regulated at some stage in the process of epithelial-to-mesenchymal transition (EMT) and this regulation may influence the energetic and migratory phenotypes of tumor cells. Taken together, these correlative analyses provide an attractive foundation for the hypothesis that dAKAP1 influences critical signaling pathways involved in cell migration and thus, through its effects on mitochondrial morphology and function, differential expression of this protein can impact metastatic tumor progression. Using our correlative studies as a guide, we classified breast cancer cell lines into two subsets: (1) the glycolytic, invasive “dAKAP1-low” and (2) the oxidative, non-invasive “dAKAP1-high” cell lines. We then used molecular biology and live-cell imaging approaches

to determine how the cells' physiology changes when dAKAP1 expression is altered. We found that dAKAP1 depletion reduced mitochondrial membrane potential and influenced mitochondrial dynamics through the regulation of mitochondrial fission in breast cancer cells. Furthermore, cells depleted of dAKAP1 and subjected to nutrient deprivation were more susceptible to decreases in viability. Conversely, increased dAKAP1 expression significantly reduced the motility of migratory cells in a PKA anchoring-dependent manner. We propose a model in which expression of dAKAP1 is temporally regulated as cancer cells progress from primary tumor to metastatic mesenchymal-like cells. Understanding how dAKAP1 expression influences mitochondrial dynamics and the migratory mechanisms of tumor cells could help serve as a foundation for future rational drug design for the prevention of dangerous metastases.

List of figures

2.1: Correlation of dAKAP1 and mesenchymal markers in breast cancer cell lines 11

2.2: Correlation of dAKAP1 and mesenchymal markers in breast cancer patient samples..... 13

2.3: Staining of primary and metastatic breast cancer tissue sections for dAKAP1 expression 15

3.1: Correlation of dAKAP1 expression with metabolism and invasion 19

3.2: Classification of “dAKAP1-high” and “dAKAP1-low” breast cancer cell lines 20

3.3: Mitochondrial membrane potential corresponds to dAKAP1 classification of cell lines 21

4.1: Schematic of dAKAP1-anchored PKA phosphorylation of the fission GTPase Drp1 24

4.2: dAKAP1-dependent phosphorylation of Drp1 to modulate mitochondrial morphology..... 26

4.3: Live-cell imaging analyses of mitochondrial dynamics 28

4.4: dAKAP1 depletion reduces membrane potential and decreases viability..... 31

5.1: dAKAP1-anchored PKA represses cell motility 35

5.2: dAKAP1-anchored PKA suppresses mitochondrial positioning to the leading edge 37

5.3: Schematic summarizing conclusions of this study..... 42

Appx. B: Un-cropped immunoblot images 70

List of tables

5.1: Phosphosites regulated with dAKAP1 overexpression in MDAMB231 cells 39

5.2: Gene ontology (GO) enrichment of phosphoproteins 40

Appx. A-1: Supplementary to figure 2.2c. Patient samples for immunoblot..... 64

Appx. A-2: Supplementary to figure 2.3. Tissue section microarray..... 64

Glossary

Abbreviation	Full name
AKAP	A-kinase anchoring protein
cAMP	Cyclic adenosine monophosphate
dAKAP1	Dual-specificity A-kinase anchoring protein 1
dAKAP1ΔPKA	Dual-specificity A-kinase anchoring protein 1 lacking PKA anchoring abilities
DAPI	4′,6-diamidino-2-phenylindole
Drp1	Dynamin-related protein 1
dsRed	*Discosoma sp*. red fluorescent protein
ECAR	Extracellular acidification rate
Eif2α	Eukaryotic translation initiation factor 2-alpha
EMT	Epithelial-to-mesenchymal transition
FCCP	Carbonyl cyanide-4-(trifluoromethoxy)phenylhydrazone
FPKM	Fragments per kilobase of transcript per million
iBAQ	Intensity-based absolute quantification (proteomics)
IDC	Invasive ductal carcinoma
ILC	Invasive lobular carcinoma
LE	Leading edge
MET	Mesenchymal-to-epithelial transition
MLI	Mitochondrial localization index
mRNA	Messenger RNA
MTS	(3-(4,5-dimethylthiazol-2-yl)-5-(3-carboxymethoxyphenyl)-2-(4-sulfophenyl)-2H-tetrazolium)
OCR	Oxygen consumption rate
OMM	Outer mitochondrial membrane
OXPHOS	Oxidative phosphorylation
paGFP	Photoactivatable green fluorescence protein
PBS	Phosphate-buffered saline
PDE	Phosphodiesterase
PKA	Protein kinase A
pSer	Phosphorylated serine
RI	PKA regulatory subunit RI (PKA type I)
RII	PKA regulatory subunit RII (PKA type II)
RMA log2	Robust multi-array average in log2 scale
siRNA	Small interfering RNA
TMRM	Tetramethylrhodamine methyl ester
TNM	TNM classification of malignant tumors (tumor, node, metastasis)
$\Delta\Psi_m$	Mitochondrial membrane potential
μm	Micrometer
nm	Nanometer

PREFACE

Portions of the text and data from this dissertation are reproduced from the following work under fair use:

Aggarwal S, Gabrovsek L, Langeberg LK, Golkowski M, Ong S-E, Smith FD, Scott JD. Depletion of dAKAP1-signaling islands during breast cancer metastasis accompanies pathological changes in mitochondrial dynamics. *Manuscript under preparation.* 2018.

Table of contents

Abstract iii

List of figures and tables v

Glossary vi

Chapter 1: Introduction 1

Chapter 2: Inverse relationship of dAKAP1 and mesenchymal markers in breast cancer 9

2.1 Introduction 9

2.2 Results 9

2.2.1 9

2.2.2 12

2.2.3 14

2.3 Conclusions 15

Chapter 3: Classification of “dAKAP1-high” and “dAKAP1-low” breast cancer cell lines 17

3.1 Introduction 17

3.2 Results 18

3.2.1 18

3.2.2 20

3.3 Conclusions 22

Chapter 4: Regulation of mitochondrial dynamics and membrane potential by dAKAP1 23

4.1 Introduction 23

4.2 Results 24

4.2.1 24

4.2.2 27

4.2.3 29

4.2.4 30

4.3 Conclusions 31

Chapter 5: Repression of cell motility and mitochondrial positioning by dAKAP1-anchored PKA 33
5.1 Introduction 33
5.2 Results 33
5.2.1 33
5.2.2 35
5.2.3 38
5.3 Conclusions 41

Chapter 6: Discussion 43

Chapter 7: Materials and methods 47

Appendix A: Description of patient samples 64
Appendix B: Un-cropped immunoblots 70
References 71

Proem

As scholars of the sciences, we have a unique opportunity to not only study the fine details of Earth and her biological mysteries, but also admire them. But “with great power comes great responsibility”, and we should use this platform to communicate science for the betterment of the vessel we’ve dedicated our lives to deciphering. Apply the knowledge we’ve had the privilege of attaining to everyday actions, with the goal of protecting the integrity of nature and leading by example. As plastic wastage clogs our oceans and toxic emissions choke our atmosphere, it’s time we do our part to convince society that human problems are not restricted to diseases of the body, but include diseases of our planet as well.

Though we travel the world over to find the beautiful, we must carry it with us or we find it not.

-Ralph Waldo Emerson (“Art” 1904)

Acknowledgements

I would like to thank John Scott for giving me the opportunity to conduct this work and for providing me with mentorship and guidance throughout my graduate career. I would also like to acknowledge my thesis committee members Shao-En Ong, Yasemin Sancak, Suzanne Hoppins, Stan McKnight, and Chris Hague. Thank you to each of you for your support, scientific insight and feedback as my project and I have evolved throughout the years. A special thank you to Joe Beavo for being an excellent mentor in the early stages of my graduate career and providing me with support, training, and inspiration that allowed me to expand not only my project, but also myself as a scientist.

To all of the members of the Scott lab, both past and present, thank you for all of the constant feedback, questions, and ideas that fueled my project and always encouraged me to persevere. A big thank you to Donelson Smith who has helped me learn how to channel my curiosity into well-developed questions that can be tested experimentally. Furthermore, thank you to all of my fellow graduate students, in particular Paula Bucko, Laura Gabrovsek, Rigney Turnham, and Janani Gopalan. Thanks for all of the coffee walks, lunch chats, and taco runs. More importantly, thanks for always supporting me not only scientifically, but also as friends.

Finally, thank you to my family scattered around the world. To my dad, Jeffrey Howarth, thank you for raising me to ask questions and stay inquisitive – you never let my child-like curiosity die. To my mom, Linda Howarth, thank you for always being willing to listen to as much or as little as I wanted to say and for always finding a way to keep me moving forward. To my little brother Neil, thank you for always being an important part of my life, no matter how far apart we are physically. To my in-laws, thank you for your love, encouragement, and faith in my pursuits. Whether it's a friendly face to talk to (Bhabhi), a compassionate soul to hear from (Bhaiyya), or genuinely caring people who only want the best for me (Papa and Mummy), I can always take comfort in the family and home I've found with you all. Lastly, thank you to my husband, Nitin. You have stood by me and supported me in every imaginable way during this journey and I can without a doubt say that none of this would have been possible without your love and your confidence in me.

Dedication

To my husband Nitin…

You're the most determined person I've ever met and I'm unbelievably lucky to have that dedication spill over into my life. You have been my only constant on this otherwise unpredictable path, and that means the world to me. Thank you for these past five years – and I can't wait to step into my future because I know, with you by my side, I am capable of anything.

To my grandfather "Grampy"…

You always knew how to keep life interesting by taking the path less traveled. You taught me the foundations of my philosophy on science: (1) that medicine and nature are one in the same and (2) to stay skeptical of what people claim until they can prove it to you.

Chapter 1:

Introduction

1.1 Molecular regulation of breast cancer progression

Approximately one in eight women will be diagnosed with breast cancer in their lifetimes. Although advances in understanding this disease have increased the likelihood of a good prognosis, 5-year survival rates plummet to just 22% for patients with metastatic (stage IV) breast cancer[1]. Therefore, elucidating molecular mechanisms that underlie this progression to metastatic disease is necessary for the development of more efficacious therapies. Onset of metastasis is often thought of as a consequence of cellular reprograming events encompassing the epithelial-to-mesenchymal transition (EMT)[2-4]. Bioinformatic analyses of mRNA and protein datasets have identified predictive elements of tumor progression that change during EMT and metastasis[5,6]. Many of these altered proteins regulate processes such as communication with the extracellular environment, cytoskeletal remodeling, and cellular metabolism that are critical to tumor cell migration and survival. Additionally, altered mitochondrial dynamics and signaling events contribute to cellular migration, a process akin to metastasis[7,8]. The role of mitochondria in the tumor environment and metastasis remains poorly understood. However, involvement in cancer signaling combined with importance to cell survival indicates that mitochondrial function may be crucial in cancer progression.

Breast cancer tumors can be classified in many ways, but are clinically resolved into four 'intrinsic' subtypes: Basal-like, HER2-enriched, Luminal A, and Luminal B[9,10]. Patients often face the risk of relapse and/or metastasis, and this risk varies per classification. Without adjuvant treatment, the HER2-enriched and Luminal B subtypes were found to be the most aggressive,

while Luminal A had the most favorable outcome[10]. Furthermore, advances in treatment have allowed the development of targeted therapies to increase prognosis of patients with this disease. For example, prognosis for patients with aggressive HER2-enriched breast cancer has been improved with the development of a monoclonal antibody drug, trastuzumab[11]. This drug was designed to induce an immune-mediated response to target the HER2 receptor and thus reduce HER2-related signaling, which normally facilitates cell growth and division. Other common treatment strategies include the use of drugs targeting the estrogen and progesterone receptors (ER and PR, respectively), which are also often enriched in primary breast tumors, to reduce cancer cell proliferation and viability[9]. Although such existing treatments are often successful in primary tumors, once the disease becomes metastatic, patient survival rates drop[1]. This places the field of breast cancer research at an interesting junction between primary breast tumors being fairly well understood with effective treatment strategies, yet after metastasis becoming a dangerous enigma. This highlights the need for new research to focus on metastatic disease and the mechanisms used by tumor cells to undergo this change to uncover targets for future anti-metastatic therapies.

1.2 Anchoring proteins in cancer

Cellular signaling orchestrates every function of living organisms; a strictly coordinated performance governed by spatial constriction and temporal cues at the molecular level. The anchoring of signaling molecules by A-Kinase anchoring proteins (AKAPs) helps to organize these events within the cell. Disruption of these tightly controlled AKAP-anchored signaling events can lead to a wide variety of diseases such as diabetes, heart disease, cataracts, and cancer[12].

Recent work on scaffolding proteins in cancer suggests that these molecules may act as distinct hubs of enzymatic activity that influence cancer cell health[13-17]. These include AKAPs, a family

of scaffolding proteins that tether the cyclic AMP (cAMP)-dependent protein kinase A (PKA) and other signaling enzymes to intracellular membranes and organelles[18,19]. The PKA holoenzyme is comprised of two catalytic subunits (C) and two regulatory subunits (R). When cAMP binds to the R subunits, the C subunits dissociate and locally phosphorylate substrates[18,19]. AKAPs interact with the R subunits of the PKA holoenzyme to anchor PKA to discrete locations, and many AKAPs have a preference for one of the two classes of regulatory subunits: RI or RII[18-20]. This specificity allows further regulation within the AKAP family to anchor unique combinations of signaling molecules within the cell. These "AKAP signaling islands" allow local control of the phosphorylation state and activity of target substrates within precisely defined microenvironments. This provides a means to not only efficiently control the relay of information within cells, but to insulate signals at defined subcellular locations to prevent indiscriminate crosstalk. Moreover, PKA signaling events contribute to the maintenance of an epithelial-like phenotype to inhibit EMT of tumor cells[21]. Combined, these observations raise the notion that PKA signaling in cancer can be differentially regulated within the cell, maintained by these "AKAP signaling islands," and influence a diverse range of cellular events.

Attention on the importance of AKAPs and PKA regulation in cancer is growing in recent times. An aberrant fusion of the PKA catalytic subunit with exon 1 of the gene for heat shock protein 40 (*DNAJB1*) was associated with enhanced PKA activity and is predicted to be oncogenic in fibrolamellar hepatocellular carcinoma (FL-HCC)[22,23]. Another somatic mutation of the PKA catalytic subunit (L205R) has been reported in cortisol-secreting adrenal adenomas, resulting in the inability to interact with the R subunits to form PKA holoenzyme, leading to constitutively active, unregulated PKA C[13,24]. The AKAP Gravin (encoded by *AKAP12*) was found to be involved in mitotic progression in various cancer types, mostly through regulatory interactions with Polo-like kinase 1 (Plk1) and Aurora A (AurA)[14,15]. Another AKAP, AKAP-Lbc (encoded by *AKAP13*), promotes mitogen-activated protein kinase (MAPK) signaling by acting as a scaffold

for growth factor responsive elements as well as anchoring local PKA to augment the Erk1/2 signaling cascade[12,25]. Furthermore, AKAPs and somatic mutations of this protein family are differentially correlated with survival, metastasis, and molecular subtype in breast cancer[16]. The involvement of this family of proteins in cancer signaling underscores their diverse functions within the cell as well as a growing interest in the regulation of these "AKAP signaling islands" as potential targets for therapeutic intervention in cancer.

1.3 Mitochondrial morphology in disease

Mitochondria are commonly known as "the powerhouse of the cell" for their role in the production of adenosine triphosphate (ATP), a molecule that provides the energy to many cellular processes. In addition to being a major site of energy metabolism, these organelles also regulate calcium signaling and calcium homeostasis, and are a key signaling hub upstream of apoptosis[26]. Since these organelles are imperative to the maintenance of normal cell health, there are various mechanisms in place to preserve their function. Mitochondria often exist as a network of interconnected organelles that can freely exchange components and metabolites as necessary[26-28]. However, the morphology and connectivity of this network is governed by many factors such as localized cellular energy needs, cell health, cell type, and environmental conditions. The balance between elongated and fragmented mitochondrial networks is known as mitochondrial fission/fusion and is controlled by a series of proteins that can either fuse mitochondrial membranes together (fusion) or break them apart (fission)[27,28]. Fused networks are often associated with enhanced mitochondrial function and decreased sensitivity to apoptotic stressors, while fission often works in concert with mitophagy and can be upstream of apoptosis[27,29]. These dynamic processes can also serve as an adaptive mechanism in a challenging environment such as hypoxia or nutrient deprivation[30-33], both of which are relevant to disease physiology, in particular the tumor microenvironment of cancer.

Dynamin-related GTPase proteins are the backbones for the balance of mitochondrial dynamics. Fusion is mediated by the mitofusins (MFN1/MFN2) located at the outer mitochondrial membrane (OMM), as well as the inner mitochondrial membrane (IMM) GTPase OPA1 (optic atrophy 1)[27,34,35]. Conversely, mitochondrial fission is largely driven by another dynamin-related GTPase, dynamin-related protein 1 (Drp1), which interacts with OMM-anchored adaptor proteins Mff, Fis1, and MiD49/51 to oligomerize and mechanically constrict mitochondrial membranes, resulting in mitochondrial fission[27,36,37]. Furthermore, localization and motility of mitochondria is supported by the interaction of cytoskeleton and molecular motors with mitochondria, such as the OMM-localized small GTPase proteins Miro1/2 (mitochondrial Rho GTPase 1/2) and TRAK (trafficking kinesin protein) family adaptor proteins[29]. Mitochondrial trafficking is further regulated by the OMM protein syntaphilin, which can directly link mitochondria to microtubules[29,38].

Spatial regulation of these dynamic processes via anchoring molecules adds another layer of complexity to the control of mitochondrial morphology. The mitochondria can be subdivided into three signaling compartments: the OMM, the IMM, and the intermembrane space (IMS). Multiple AKAPs have been reported at each of these mitochondrial compartments, creating distinct cAMP/PKA signaling hubs by sequestering unique assortments of interacting proteins[39]. Since the OMM serves as a physical barrier separating the inner workings of the mitochondria from the rest of the cell, proteins at this location can act as gatekeepers and important regulators. The OMM-localized AKAP, dAKAP1 (encoded by *AKAP1*, discussed further below), is responsible for sequestering a variety of signaling molecules to influence mitochondrial membrane potential and fission[40-42]. Although cAMP/PKA signaling within the mitochondria is disputed, AKAPs have been observed at the IMM and IMS of this organelle[43-45]. A key regulator of mitochondrial fusion and cristae maintenance, the dynamin-related GTPase OPA1 was identified as an AKAP and is located in the IMS via association with the IMM[46-48]. Furthermore,

the RI-specific AKAP SKIP (sphingosine kinase interacting protein) was also found in the IMS, further suggesting a functional role for cAMP/PKA signaling within this tightly controlled organelle[49,50].

Tumor cells grow and proliferate rapidly. Consequently, the demand for nutrients often exceeds environmental availability due to the unregulated growth and the insufficient access to vascular supply. However, cancer cells can counter these harsh conditions via modulation of metabolism[31]. Serum starvation of cancer cells in culture can be thought of as a physiologically appropriate method to induce metabolic stress, forcing cells to adapt as they would in the *in vivo* tumor environment[31,33]. Mitochondria elongate during serum starvation and this process has been tied to enhanced cell viability and protection of mitochondria from mitophagy during times of metabolic stress[32,33]. This protective mitochondrial elongation observed with serum starvation is attributed to the inhibition of the fission GTPase Drp1 via phosphorylation at Ser637[32,33].

Moreover, changes in mitochondrial morphology have been linked to migration and invasion of cancer cells. Fragmented mitochondria appear to favor cell migration, and this fragmentation is due primarily to the activity of Drp1[51]. Conversely, elongated and interconnected mitochondrial networks inhibit migration[51,52]. Although a mechanistic connection between mitochondrial morphology and cell motility remains unknown, we postulate that smaller mitochondria are more easily trafficked to the leading edge (LE) of migrating cells to facilitate local energy production. Interestingly, alternative splicing of the OMM-microtubule associated protein syntaphilin has been associated with enhanced mitochondrial trafficking during cancer cell migration under hypoxic conditions[53]. Moreover, both AMP-activated protein kinase (AMPK) and PKA signaling at the leading edge is required for cellular migration, and inhibition of either of these kinases at the LE hinders migration[54,55]. Further evidence suggests that not only the activity, but also the anchoring of PKA to an AKAP is required for this process[55]. Interestingly, the mitochondrial

dAKAP1 was identified as an AMPK substrate, further suggesting cross talk between these two signaling pathways[56].

1.4 Relevance of dAKAP1 to mitochondrial morphology and anchored signaling in disease

This outer mitochondrial AKAP, dAKAP1 (also known as AKAP1, D-AKAP1, AKAP121, AKAP149, S-AKAP84), was originally discovered as an OMM-targeted AKAP in male germ cells and later described as a dual-specificity AKAP that can sequester both type I and type II PKA holoenzymes[57,58]. Expression of dAKAP1 is reported to be neuroprotective in primary neurons and cerebral tissue subjected to pro-apoptotic treatment[59,60]. Moreover, dAKAP1 deficiency sensitized cardiac tissue to damage in response to cardiac insult[61,62]. These studies largely attribute changes in apoptotic susceptibility to dAKAP1's regulation of mitochondrial health, since decreases in oxidative metabolism and swollen or abnormal mitochondrial morphologies have been observed in cells with decreased expression[59-62]. Additionally, depletion of dAKAP1 in cells impaired oxidative metabolism and reduced tumor size when subsequently injected into the brain of nude mice[17]. Taken together, these data suggest that dAKAP1 is critical for mitochondrially-regulated survival mechanisms via changes in mitochondrial morphology, metabolic function, and signaling.

Furthermore, dAKAP1 also sequesters a variety of interacting partners to the OMM. These include Protein Phosphatase 1 (PP1)[42,63], the cAMP-degrading phosphodiesterase 4a (PDE4a)[64], and the microtubule-associated Rho guanine exchange factor and oncoprotein Lfc[65,66]. These diverse binding partners of dAKAP1 provide the potential for bi-directional control of cAMP/PKA signaling localized at the OMM by anchoring not only PKA, but also enzymes that regulate PKA phosphorylation.

Additionally, dAKAP1 has been established as an important regulator of the inhibitory phosphorylation of Ser637 on Drp1 to prevent mitochondrial fission[40,41,60]. As previously discussed, this PKA-regulated phosphorylation event is important for cell response to serum starvation[32,33]. Fragmented mitochondrial morphology supports breast cancer cell migration and invasion, and these morphological changes are also directly tied to Drp1 activity[51,52]. Moreover, anchored PKA activity at the leading edge (LE) of a migrating cell is required for efficient migration[55]. These findings poise dAKAP1 at an interesting locus between mitochondrial morphology, metabolism, and cell migration. Expression of dAKAP1 seems to have opposing effects on both cancer-related 'favorable' features of cell viability and cell motility. This suggests that dAKAP1 expression may be temporally regulated in cancer cells to influence these processes as required by their environment.

In this study, we describe an inverse relationship between dAKAP1 levels and a mesenchymal expression profile. We propose that decreases expression of this mitochondrial anchoring protein in tumors accompanies molecular and cellular changes that promote metastasis in breast cancer. Although dAKAP1 expression is protective from cell death[59,60], changes in mitochondrial morphology associated with lower levels of this protein also facilitate migration[51,52,62]. Therefore, we propose a model in which levels of this anchoring protein are temporally controlled by tumor cells as they progress from primary tumor toward metastasis, analogous (or concurrent) with expression profile alterations as cells undergo EMT (see also fig. 5.3, discussed in Chapters 5 & 6). Recent support for this concept comes as dAKAP1 is differentially expressed between breast cancer molecular subtypes, suggesting that dAKAP1 may play distinct roles determined by tumor signaling environment[16].

Chapter 2:

Inverse relationship of dAKAP1 and mesenchymal markers in breast cancer

2.1 Introduction

Although advances in understanding breast cancer signaling have increased the likelihood of a good prognosis, 5-year survival rates plummet for patients with metastatic disease[1]. Therefore, understanding cellular mechanisms that are associated with disease progression is essential to the development of new rationally designed therapies. In particular, a cellular reprogramming event known as the epithelial-to-mesenchymal transition (EMT) is often thought to accompany metastasis[2-4]. Since AKAP family members are known to regulate oncogenic events in some cancers[12,15], we postulate that this protein family may be important to localized cellular signaling in breast cancer disease progression. By calculating the correlation between expression of various AKAPs and that of EMT markers, we identified a striking inverse correlation between the mitochondrial dAKAP1 and markers of EMT (results detailed in 2.2, below). Because of its role in regulating mitochondrial health and morphology, this dAKAP1-EMT marker relationship was further investigated for a physiological role in breast cancer metastatic progression.

2.2 Results

2.2.1 Relationship of dAKAP1 and mesenchymal markers in breast cancer

To explore the potential relationship between AKAPs and mesenchymal markers[5] in breast cancer, a comprehensive examination of mRNA expression data from the Cancer Cell Line Encyclopedia (CCLE) was conducted[67] (figs. 2.1a & b). Expression level of dAKAP1 was compared to that of 36 markers that have been experimentally validated as up-regulated when cells undergo EMT[5,6]. One striking observation was a strong negative correlation between

expression of mesenchymal markers and the mitochondrial anchoring protein dAKAP1 (also called *AKAP1*; figs. 2.1a & b). Conversely, Gravin (encoded by *AKAP12*) displayed a strong positive correlation, suggesting that differential subcellular targeting of PKA may influence opposing pathways in breast cancer progression. Based on these results, we chose to focus on dAKAP1 due to its role at the mitochondria, as reprogramming of cellular energy homeostasis is a hallmark of cancer and is related to alterations in mitochondrial structure and metabolism[7,8,68].

The negative correlation between dAKAP1 mRNA levels and average mesenchymal marker expression persisted across the 59 breast cancer cell lines represented in the CCLE (Pearson's r=-0.74; figs. 2.1c & d). Furthermore, a similar inverse relationship with dAKAP1 was also apparent across a variety of cancer etiologies, suggesting that dAKAP1's relationship to mesenchymal markers is conserved in multiple cancer types (figs. 2.1e & f). Based on these analyses, we postulate that dAKAP1 levels drop as cells adopt a mesenchymal, metastatic phenotype.

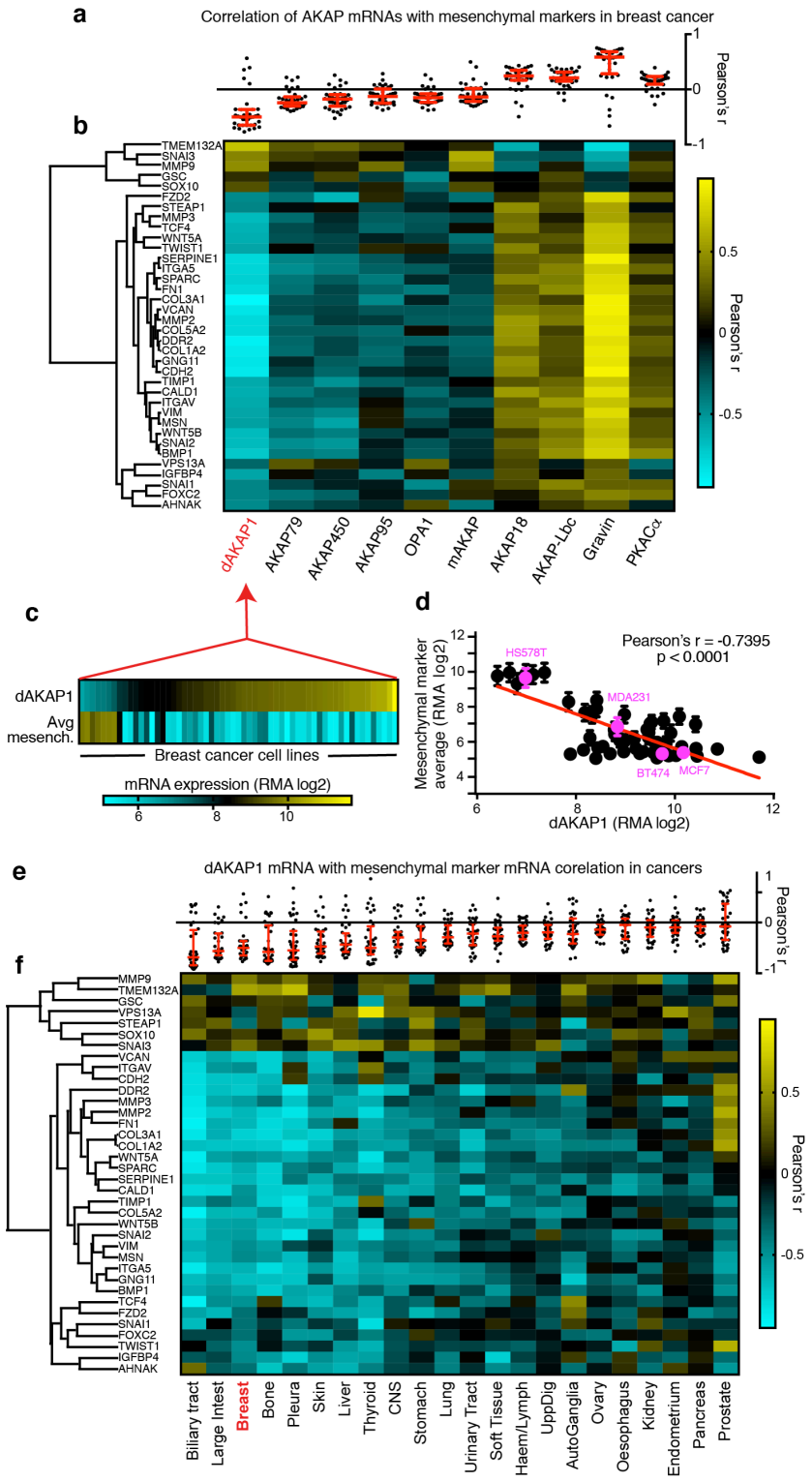

Figure 2.1. Correlation of dAKAP1 and mesenchymal markers in breast cancer. (a) Pearson's r values of the correlation of selected AKAPs and PKA catalytic subunit mRNA with 36 mesenchymal markers from gene array analysis data of CCLE breast cancer cell lines (n=59 cell lines)[67]. Median and interquartile ranges (red bars) are indicated. **(b)** Heat map of Pearson's r values between AKAPs and individual mesenchymal markers as in (a). Rows (mesenchymal genes) were organized with hierarchical

clustering, columns (AKAPs) are organized by mean r value. Intensity scale indicates Pearson's r values ranging from high (yellow) to low (teal). **(c)** Heat map of dAKAP1 mRNA and mean mesenchymal marker mRNA expression across each individual 59 breast cancer cell line used in this dataset, organized by ascending dAKAP1 mRNA expression. **(d)** Scatter plot of dAKAP1 mRNA against mean mesenchymal marker mRNA in the 59 breast cancer cell lines shown in (c). Error bars represent s.e.m. Breast cancer cell lines MCF7, BT474, MDA231 (also called MDAMB231), and HS578T used later in this study are highlighted in magenta. **(e)** Pearson's r values of the correlation of dAKAP1 and mesenchymal marker mRNA from gene array analysis data of CCLE cancer cell lines, separated by cancer etiology (n=1,037 cell lines). Median and interquartile ranges (red bars) are indicated. **(f)** Heat map of Pearson's r values between dAKAP1 and individual mesenchymal markers as in (e). Rows (mesenchymal genes) were organized with hierarchical clustering, columns (cancer etiology) are organized by mean r value. Intensity scale indicates r values ranging from high (yellow) to low (teal).

2.2.2 dAKAP1 is negatively correlated with mesenchymal markers in patient samples

Further analysis was performed to investigate if this negative correlation was maintained in *in vivo* patient tumors. Primary breast cancer tumors can be classified in several ways, but are clinically resolved into four subtypes: Basal-like, HER2-enriched, Luminal A, and Luminal B[10,69,70]. Using this convention, we examined both mRNA and protein levels in data sets generated from patient samples[70] (figs. 2.2a & b). Again, dAKAP1 expression was negatively correlated with the appearance of mesenchymal markers. Notably, negative correlations were observed in each breast cancer subtype, but were particularly evident in the basal and HER2 classifications (figs. 2.2a & b). This suggests that reduction in this anchoring protein is a general phenomenon as breast cancer cells transition toward a mesenchymal phenotype, and is conserved from patient samples to cultured cell lines.

Immunoblot analysis of primary tumor lysates obtained from four patients provided experimental validation of this observed trend (fig. 2.2c; samples defined in appx. A-1). Samples were arranged to cover a range of dAKAP1 protein levels, in descending order (fig. 2.2c; top panel). E-cadherin identified tumor samples rich in epithelial markers (fig. 2.2c, second panel), whereas N-cadherin and the transcription factor Snail were mesenchymal markers[5] (fig. 2.2c, third and fourth panels). Detection of Eif2α served as a loading control (fig. 2.2c, bottom panel). Strong

immunoblot detection of dAKAP1 expression correlated with lower levels of the mesenchymal markers N-cadherin and Snail (fig. 2.2c, top, middle and mid-lower panel, patient A & B). Conversely, reduced detection of dAKAP1 was coupled to an enrichment of these mesenchymal markers (fig. 2.2c, top, third and fourth panels, patient C & D). This provides experimental evidence that decreased dAKAP1 levels are associated with the appearance of the mesenchymal markers N-cadherin and Snail in clinical samples from breast cancer patients. Taken together, these analyses provide a solid foundation for the hypothesis that dAKAP1 levels are reduced as breast cancer cells adopt a mesenchymal phenotype, often associated with metastatic progression.

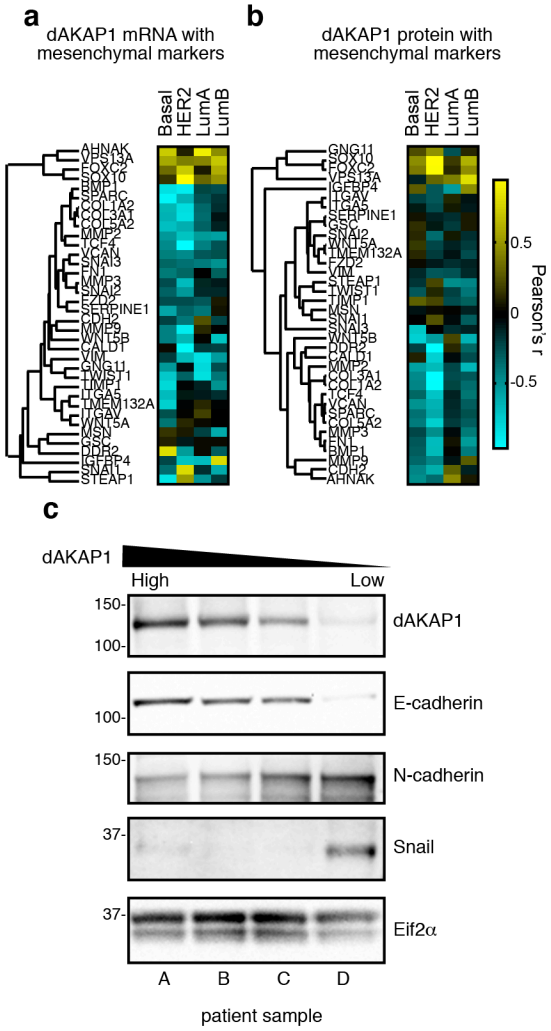

Figure 2.2. Correlation of dAKAP1 and mesenchymal markers in breast cancer patient samples. Heat maps depicting correlation of mesenchymal marker expression with **(a)** dAKAP1 mRNA and **(b)** dAKAP1 protein expression from breast cancer patient samples (n=77 TCGA patient samples)[70] separated by the four clinically defined breast cancer subtypes (columns, indicated above each lane). Rows (mesenchymal genes) were organized with hierarchical clustering. Intensity scale indicates Pearson's r values ranging from high (yellow) to low (teal). **(c)** Immunoblot analysis of patient samples from breast cancer tumors monitoring dAKAP1 expression (top); E-cadherin epithelial marker (second); N-cadherin and Snail (third & fourth, respectively) mesenchymal markers and (bottom) Eif2α loading control. Individual patients are designated A-D at the bottom of the panel.

2.2.3 Expression of dAKAP1 is reduced in tumor cells after metastasis

The *in vivo* tumor microenvironment contains two key elements: tumor cells and stromal cells[71-73]. In some cancers, stromal cells utilize glycolytic metabolism to fuel the tumor cells with intermediate metabolites to thereby support cancer cell survival[71]. Accordingly, expression of dAKAP1 is elevated in primary breast tumors that exhibit this type of metabolic environment[72,73]. We postulate that dAKAP1 facilitates metabolic changes at the mitochondria, whose function is not only crucial for cell survival, but also essential to meet the high energy demands associated with cancer.

Since changes in metabolism accompany EMT and metastasis in tumors[7,8], we sought to establish if levels of dAKAP1 were changed after metastasis had occurred. Levels of dAKAP1 were quantified in an array of 45 paired primary and metastatic breast cancer tumors (samples defined in appx. A-2). Analysis of a representative tissue pair is shown in figures 2.3a-f. Staining in tumor cells (figs. 2.3a & d, shaded regions) was compared to the surrounding stroma. Detection of dAKAP1 (green) and counterstaining with the nuclear marker DAPI (blue) revealed the tissue distribution of this anchoring protein (figs. 2.3b & e). A signal intensity heat gradient was used to visualize dAKAP1 protein levels in these compartments (figs. 2.3c & f). Strong dAKAP1 staining in tumors was evident in 60% of primary tumor samples (fig. 2.3g, yellow). In contrast, only 42% of the corresponding metastatic tumor sections exhibited robust expression of the anchoring protein (Fig. 2.3h, yellow). Only 4% of primary breast tumors were scored as weakly expressing dAKAP1 as compared to 22% of the paired metastatic tumors (fig. 2.3g & h, teal). Thus, we conclude that dAKAP1 expression is reduced after cells have undergone metastasis. We postulate that this decreased expression in tumor cells is associated with a molecular environment that supports metastasis.

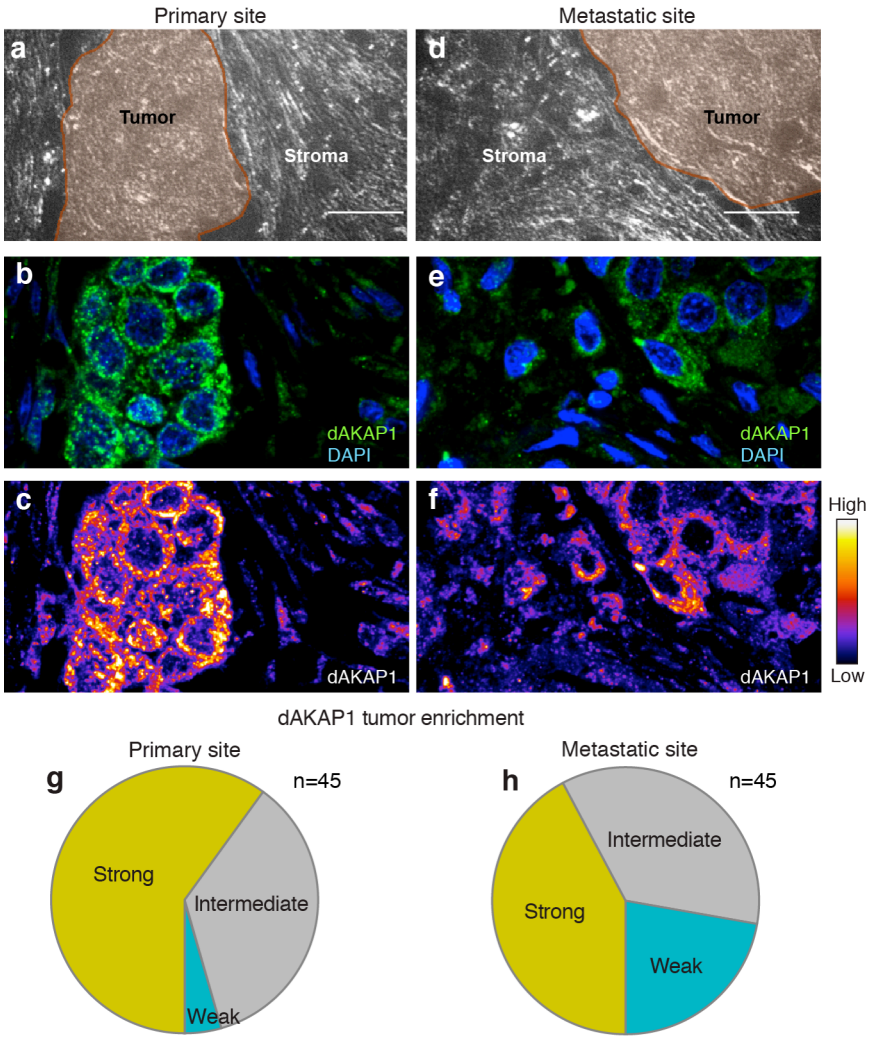

Figure 2.3. Staining of primary and metastatic breast cancer tissue sections for dAKAP1 expression. (a) Representative images from either primary tumor **(a, b, c)** or site of metastasis **(d, e, f)**. **(a)** & **(b)** Brightfield images of tissue sections. Tumor regions are shaded in brown. **(c)** & **(d)** Immunofluorescent detection of dAKAP1 (green) and nuclei (DAPI, blue). **(c)** & **(f)** signal intensity of dAKAP1 staining is visualized by pseudocolor heat gradient. Amalgamated data of 45 primary **(g)** and metastatic **(h)** tumor sections quantifying tumor signal enrichment of dAKAP1 staining. Strong (yellow), intermediate (grey), and weak (teal) signals are categorized.

2.3 Conclusions

Results presented in this chapter introduce an inverse relationship between dAKAP1 and mesenchymal marker expression. Although such relationships were not apparent across all AKAPs, the AKAP Gravin also appeared to be related to mesenchymal expression but,

conversely, was strongly positively correlated (fig. 2.1). The inverse relationship between dAKAP1 and mesenchymal markers is fairly well conserved in breast cancer, from cell lines (fig. 2.1) to patient samples (fig. 2.2). Correlative analysis and experimental evidence in patient samples appears to be, to some extent, regulated by molecular subtype of the tumor. Particularly at the level of protein expression, dAKAP1 is most strongly inversely related to a subset of mesenchymal markers in HER2 positive breast cancer tumors (fig. 2.2). Taken together, these findings are indicative of dAKAP1 expression being decreased in cell types more likely to adopt a mesenchymal expression profile and progress toward a migratory phenotype.

Furthermore, analysis of 45 paired primary and metastatic tumor sections identified a modest decrease in dAKAP1 expression after metastasis (fig. 2.3). Results from this chapter form the basis for our model that: (1) dAKAP1 expression is reduced in certain tumor cells during metastasis, (2) maintained at low levels while cells are migratory, and (3) increased back, but to a lesser extent, once cells have seeded the metastatic site. Molecular mechanisms are investigated in later chapters to explore cellular processes that may be influenced by changes in dAKAP1 expression during this progression.

Chapter 3:

Classification of "dAKAP1-high" and "dAKAP1-low" breast cancer cell lines

3.1 Introduction

Highly proliferative tumor cells often exhibit enhanced glycolytic metabolism (known as the Warburg effect). However, more recent studies show that this metabolic shift is often reversible and that aerobic respiration is also critical for successful metastasis and survival of cancer cells[7,8]. Furthermore, dAKAP1 has been implicated with changes in metabolism in glioblastoma cells[17] and depletion of this protein is linked to decreases in mitochondrial membrane potential, a feature indicative of normal respiratory chain function[42,74]. We hypothesized that dAKAP1 levels influence metabolic processes important for breast cancer cell health and metabolism, and may therefore effect breast cancer progression by modifying these functions.

Additionally, cellular migration and invasion are processes commonly used as surrogates for the metastatic potential of cancer cells[75]. Moreover, breast cancer cell lines associated with more aggressive phenotypes are often more glycolytic than their non-invasive counterparts[76]. Therefore, in understanding a role for dAKAP1 in breast cancer metastasis, both metabolism and cellular invasion were of interest. *In silico* comparison of reported dAKAP1 levels to published values for both metabolism and invasion revealed a separation among breast cancer cell lines that afforded classification as either "dAKAP1-high" or "dAKAP1-low" (results detailed in section 3.2). This separation further supported the hypothesis that dAKAP1 is biologically relevant to cell health and mitochondrial physiology as it relates to metastatic breast cancer progression.

3.2 Results

3.2.1 Levels of dAKAP1 are associated with motility and mitochondrial function

Since altered glycolytic metabolism and increased cell motility are hallmarks of metastatic tumor progression[7,8,68,75,76], we analyzed published data sets to investigate if levels of dAKAP1 are linked to either process. Values for metabolic phenotype were determined as the reported ratio of oxygen consumption rate (OCR) to extracellular acidification rate (ECAR) for each cell line, as assessed by SeaHorse assay[76]. Comparison of dAKAP1 levels to metabolic phenotype revealed that cell lines that were more glycolytic (low OCR/ECAR ratio) had lower levels of dAKAP1 protein expression[76,77] (fig. 3.1a, yellow). Conversely, cell lines that were more aerobic (high OCR/ECAR ratio) tended to have greater levels of dAKAP1 expression (fig. 3.1a, grey). In parallel, we compared dAKAP1 expression to reported values of invasive potential evaluated by transwell assay[75,77] (fig. 3.1b). Again, dAKAP1 was markedly reduced in the most invasive cancer cell lines (fig. 3.1b, yellow). These analyses suggest that breast cancer cell line metabolic and migratory phenotypes are related to dAKAP1 expression level. Therefore, we classified breast cancer cell lines into two groups: *"*dAKAP1-high*"* lines (grey), including MCF7 and BT474, that are metabolically oxidative and non-invasive; and *"*dAKAP1-low*"* lines (yellow), including MDAMB231 and HS578T, that are glycolytic and motile. This classification was also observed at the level of mRNA expression (fig. 3.1c & d).

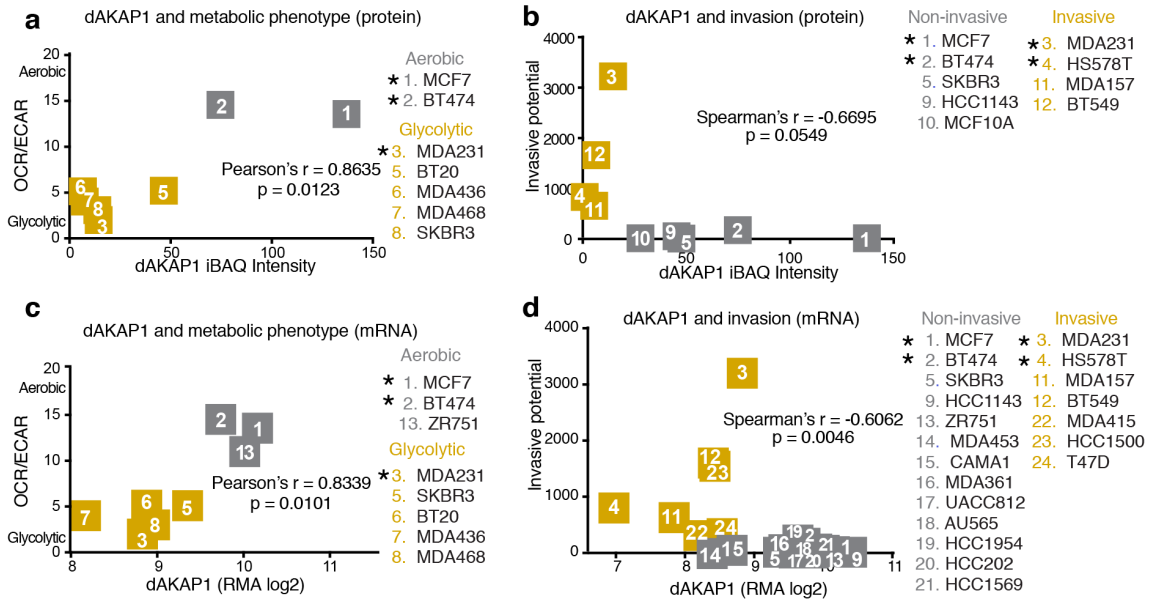

Figure 3.1. Correlation of dAKAP1 expression with metabolism and invasion. Scatter plots comparing dAKAP1 iBAQ protein expression[77] to **(a)** metabolic analysis of aerobic respiration (OCR)/glycolysis (ECAR)[76]. Cell lines designated as predominantly glycolytic (yellow) or aerobic (grey) are indicated. **(b)** Comparison to invasive potential assessed by transwell assay[75]. Invasive (yellow) and non-invasive (grey) cell lines are indicated. Scatter plots comparing dAKAP1 mRNA expression[67] to **(c)** metabolic analysis of OCR/ECAR[76]. Cell lines designated as predominantly glycolytic (yellow) or aerobic (grey) are indicated. **(d)** Comparison to invasive potential assessed by transwell assay[75]. Invasive (yellow) and non-invasive (grey) cell lines are indicated. Cell lines used experimentally are marked with an asterisk. Pearson's (linear, OCR/ECAR) or Spearman's r (non-linear, invasion) and respective p values are indicated.

Immunoblot analysis of lysates from each of the four representative breast cancer cell lines experimentally established that detection of dAKAP1 expression followed the predicted trend (figs. 3.2a, top panel). Quantification of data from three independent experiments confirmed that dAKAP1 protein is reduced in the invasive cell lines (fig. 3.2b, yellow columns). Immuno-fluorescent imaging of dAKAP1 (green) in fixed cells revealed a reticular staining pattern consistent with the mitochondrial outer membrane and signal intensity in each cell line mirrored our "dAKAP1-high" and "dAKAP1-low" designations (fig. 3.2c). These cell lines are utilized in the remainder of this study to investigate how dAKAP1 signaling at the mitochondria impacts cell motility.

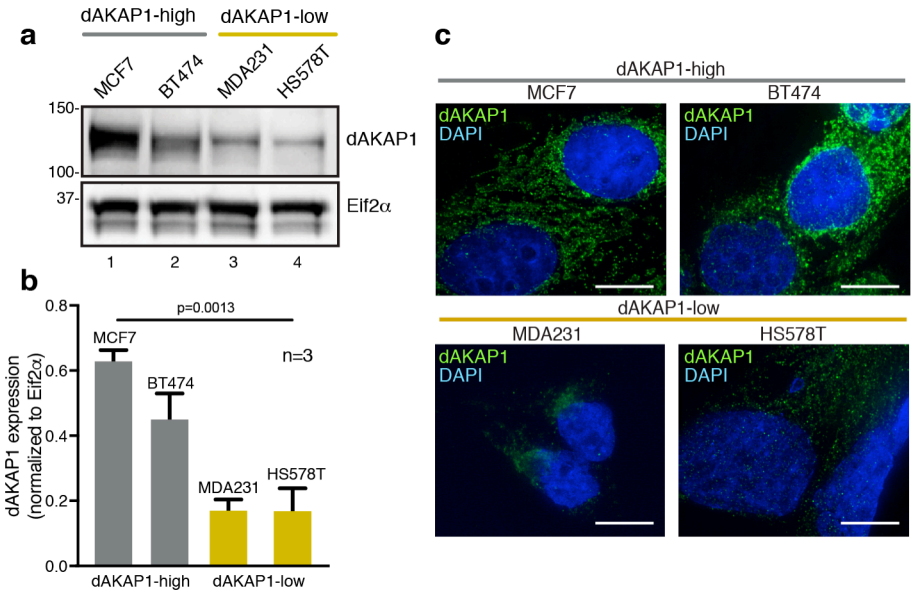

Figure 3.2. Classification of "dAKAP1-high" and "dAKAP1-low" breast cancer cell lines.
(a) Immunoblot analysis of dAKAP1 (top) levels and Eif2α (bottom) loading control in representative breast cancer cell lines. **(b)** Quantification of amalgamated data (n=3 independent blots) by densitometry. Error bars represent s.e.m. Statistical significance was determined by ordinary one-way ANOVA ($p=0.0013$; $F(3, 8)=14.76$). MCF7 and BT474 cells (grey) were designated "dAKAP1-high". MDA231 (also called MDAMB231) and HS578T (yellow) cells were designated "dAKAP1-low". (See also fig. 2.1d, magenta points.) **(c)** Immunofluorescent detection of dAKAP1 (green) and nuclei (DAPI, blue) in each cell line. Scale bars (10μm) are indicated.

3.2.2 Endogenous dAKAP1 expression is associated with mitochondrial membrane potential

As previously discussed, dAKAP1 sequesters second messenger responsive enzymes to coordinate local signaling events at the outer mitochondrial membrane, including PKA modulation of mitochondrial membrane potential ($\Delta\Psi_m$)[58,78,79]. Measurement of $\Delta\Psi_m$ serves as a gauge of respiratory chain function (OXPHOS) and an index of mitochondrial health[80-82]. Therefore, mitochondrial membrane potential was determined in the four representative breast cancer cell lines by the ratio of tetramethylrhodamine (TMRM; fig. 3.3a) to Mitotracker green FM signal intensity (fig. 3.3b). The cationic fluorophore TMRM accumulates strongly in the matrix of highly negatively charged mitochondria, a consequence of high mitochondrial membrane

potential related to OXPHOS[80]. Conversely, Mitotracker green FM is a non-membrane potential-dependent mitochondrial dye. Amalgamated data reveal that $\Delta\Psi_m$ values are reduced in the "dAKAP1-low" cell lines MDAMB231 and HS578T (fig. 3.3c & d). Thus we propose that dAKAP1 expression supports mitochondrial membrane potential and, consequently, decreased expression of this anchoring protein may disrupt respiratory chain function.

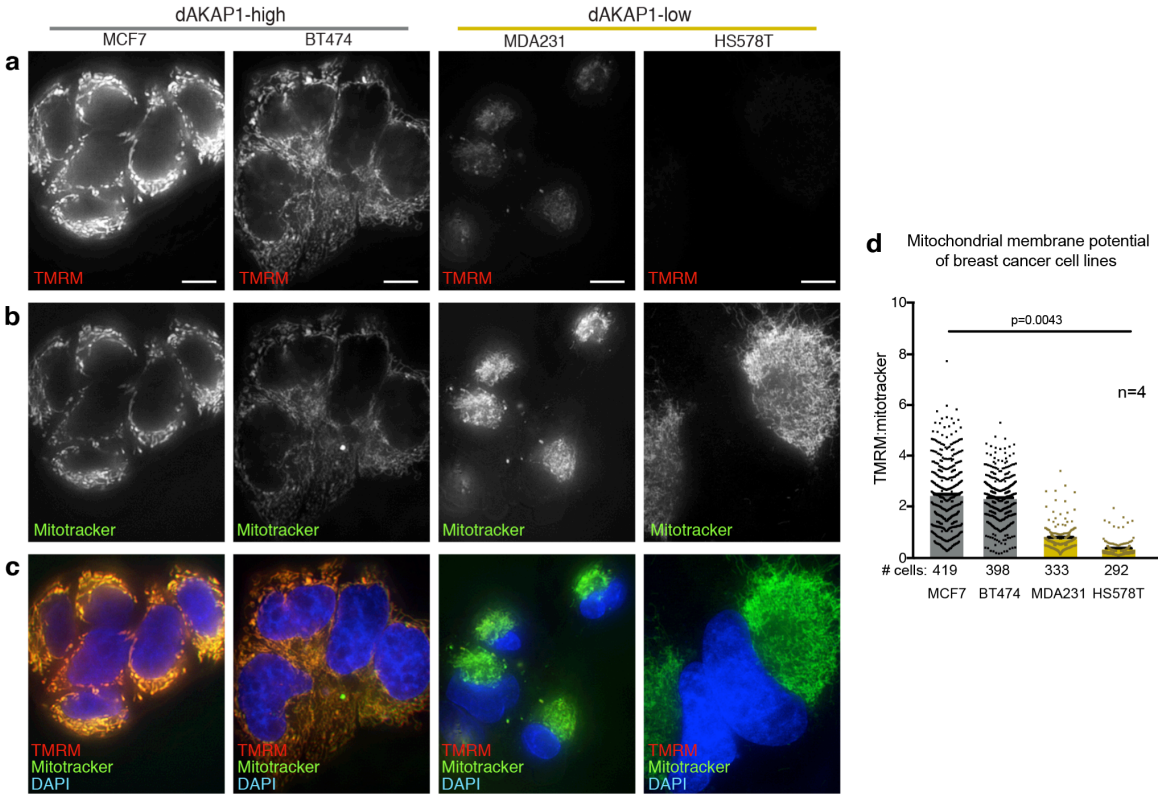

Figure 3.3. Mitochondrial membrane potential corresponds to dAKAP1 classification of cell lines. Mitochondrial membrane potentials were quantified as the ratio of **(a)** TMRM to **(b)** Mitotracker Green FM fluorescence in each cell line. **(c)** Composite images reveal elevated mitochondrial membrane potentials in "dAKAP1-high" cell lines. Scale bars (10μm) are indicated. **(d)** Quantification of amalgamated data (n=4 independent experiments). Number of cells used in analyses is listed below each column. Error bars represent s.e.m. Statistical significance was determined by one-way ANOVA (p=0.0043; F(3, 12)=7.523).

3.3 Conclusions

In this chapter, we explored the relationship of dAKAP1 with phenotypes relevant to breast cancer and breast cancer progression. Breast cancer cell lines were classified by dAKAP1 expression based on their segregation into two distinct categories: non-invasive, metabolically oxidative "dAKAP1-high" cells and the invasive, metabolically glycolytic "dAKAP1-low" cells (fig. 3.1). We went on to validate these categories experimentally in four representative cell lines, which closely followed the expected levels of dAKAP1 expression (fig. 3.2). Imaging with TMRM uncovered an analogous trend in $\Delta\Psi_m$, where mitochondrial membrane potential is significantly lower in "dAKAP1-low" cell lines than their "dAKAP1-high" counterparts (fig. 3.3). These results, combined with reports on dAKAP1 expression in other cell types[17,42], suggest a relationship between expression of this anchoring protein with maintenance of mitochondrial health, OXPHOS, and mitochondrial membrane potential.

We therefore postulate that dAKAP1 not only correlates with the phenotypes of oxidative metabolism and migration, but also has an active role in these processes. When combined with the findings from Chapter 2, our results suggest that dAKAP1 levels vary between breast cancer cell lines, reflective of variable phenotypes of cells within a tumor. Further investigation is needed to explore how these phenotypes might influence metastatic progression, and how dAKAP1 might be involved in this process.

Chapter 4:

Regulation of mitochondrial dynamics and membrane potential by dAKAP1

4.1 Introduction

The opposing processes of fission and fusion control mitochondrial morphology. The GTPase Drp1 will bind to outer mitochondrial membrane-bound adaptor proteins and oligomerize, resulting in the mechanical constriction of mitochondrial membranes known as fission[27]. This fission enzyme can be inhibited by phosphorylation at multiple sites[83]. The inhibitory phosphorylation of Ser637 on Drp1 is largely attributed to the kinase PKA[83]. Furthermore, dAKAP1-anchored PKA locally regulates mitochondrial fission by positioning the kinase at the outer mitochondrial membrane (OMM)[60,61]. Overexpression of this anchoring protein causes the interconnection and elongation mitochondrial networks largely through the phospho-Ser637 inhibition of Drp1-mediated fission, allowing unopposed fusion[59,60]. This elongated, interconnected morphology of mitochondria associated with dAKAP1 expression was also found to be protective against cell death in a PKA-dependent manner[59,60]. We postulate that the "dAKAP1-low" motile cells may be more susceptible to stress since the reduced abundance of dAKAP1 may prevent cells from employing these pro-survival pathways related to mitochondrial morphology and function. This is particularly important since "dAKAP1-low" cell lines are typically more invasive and therefore more likely to represent metastatic cells (Chapter 3). Understanding mechanisms that can sensitize metastatic cells to stress can be important for the development of rational treatment strategies. We aimed to study the influences of altered dAKAP1 expression in the context of breast cancer to better understand how mitochondrial signaling influences the phenotypic differences observed in these cells.

4.2 Results

4.2.1 Mitochondrial morphology is altered by dAKAP1 expression in breast cancer cells

Mitochondrial morphology reflects a dynamic equilibrium between the opposing actions of mitochondrial fission and fusion[27,84]. The size of mitochondria and distribution within the cell can be indicative of localized energy demand[85-87]. Motile breast cancer cells often contain smaller, fragmented mitochondria[51]. This fragmented mitochondrial network is thought to promote mitochondrial trafficking to the leading edge (LE) during the energetically taxing process of cell migration[51,52]. This process can be inhibited by the phosphorylation of the mitochondrial fission enzyme Drp1 at multiple sites, including the PKA-regulated site Ser637 (fig. 4.1)[88].

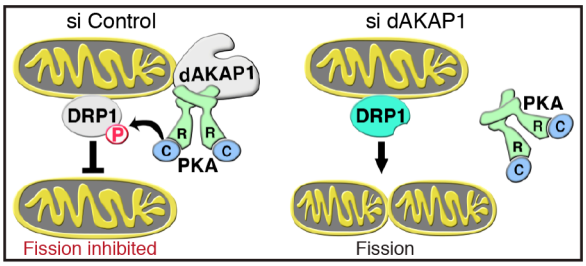

Figure 4.1. Schematic of dAKAP1-anchored PKA phosphorylation of the fission GTPase Drp1. (Left) Expression of dAKAP1 anchors PKA to the outer mitochondrial membrane, allowing phosphorylation of Drp1 to inhibit mitochondrial fission. (Right) Gene silencing of dAKAP1 reduces dAKAP1 levels, therefore allowing uninhibited fission.

In tumors, the cells in the dense center often lack access to nutrients, making this treatment condition biologically relevant to breast cancer tumor models[33]. Furthermore, mitochondrial morphology differs between the tumor edge and the tumor center, where mitochondria are more elongated[33]. Additionally, in cultured cells, serum starvation induces metabolic stress via nutrient depletion and has been found to suppress fission through the phosphorylation of Drp1 at Ser637[32,41]. Under serum starvation conditions, mitochondria elongate in a phospho-Ser637 dependent manner[32,33].

The proximity of dAKAP1-associated PKA at the outer mitochondrial membrane paired with its established role in Drp1 Ser637 phosphorylation makes it an ideal candidate to catalyze this inhibitory phosphorylation event under serum starvation conditions (fig. 4.1). Gene silencing in the "dAKAP1-high" MCF7 cell line confirmed this notion (fig. 4.2). Cells were treated with control or dAKAP1-selective siRNAs and depletion of the anchoring protein from cell lysates was confirmed by immunoblot (fig. 4.2a, top panel). Phospho-peptide antibodies were used to evaluate phosphorylation status of Ser637 of Drp1. In control cells, serum starvation enhanced the phospho-Ser637 signal (fig. 4.2a, second panel, lane 2). However, this effect was lost upon siRNA depletion of the anchoring protein (fig. 4.2a, second panel, lane 4). Immunoblot detection of total Drp1 and Eif2α served as loading controls for these experiments (fig. 4.2a, third & bottom panels). Densitometric analysis of blots from five independent experiments corroborated these results (fig. 4.2b). Therefore, we can conclude that gene silencing of dAKAP1 diminishes the phosphorylation of Ser637 on Drp1 to block serum starvation-induced inhibition of mitochondrial fission.

Concomitant changes in mitochondrial morphology were evaluated by live-cell imaging of MCF7 cells loaded with Mitotracker Green FM (figs. 4.2c-f). As anticipated, mitochondrial networks were interconnected and extended in serum-starved cells treated with control siRNA. (fig. 4.2c). This morphological change is particularly evident when visualized at higher magnification (fig. 4.2c inset). In contrast, mitochondria were fragmented in cells treated with dAKAP1 siRNA (fig. 4.2d & inset). Quantitative analyses of >100 cells under each condition confirmed that mitochondrial length (fig. 4.2e, yellow) and mitochondrial connectivity (fig. 4.2f, yellow) were reduced upon depletion of this anchoring protein.

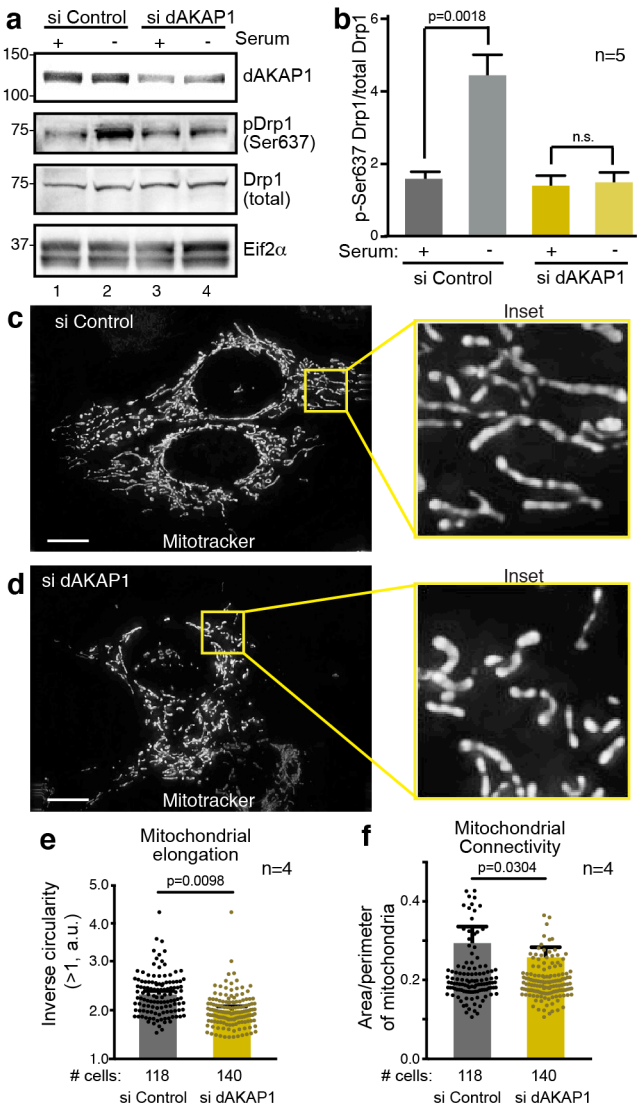

Figure 4.2. dAKAP1 facilitates phosphorylation of Drp1 to modulate mitochondrial morphology. **(a)** siRNA depletion of dAKAP1 suppresses phosphorylation of Ser637 on Drp1. Immunoblot detection of dAKAP1 (top); pDrp1-Ser637 (second); total Drp1 (third); and Eif2α (bottom) loading control. Analysis of MCF7 cells treated with si Control (lanes 1 & 2), siRNA against dAKAP1 (lanes 3 & 4). Samples in lanes 2 and 4 are serum starved. **(b)** Quantification of amalgamated data (n=5 independent blots) by densitometry. Error bars represent s.e.m. Statistical significance was determined by two-tailed Student's t-test. **(c-f)** Fluorescence detection of Mitotracker Green FM to monitor mitochondrial morphology in MCF7 cells treated with **(c)** si Control or **(d)** siRNA against dAKAP1. Scale bars (10μM) are indicated. Insets reveal selected 10μM regions at higher magnification. Quantification of **(e)** mitochondrial elongation and **(f)** mitochondrial connectivity in si Control (grey) and si dAKAP1 (yellow) treated cells (n=4 independent experiments). Number of cells used in each analysis is indicated below each column. Error bars represent s.e.m. Statistical significance was determined by two-tailed Student's t-test.

4.2.2 Mitochondrial dynamics are hindered with dAKAP1 with depletion

Dispersal of mitochondrially-targeted photoactivatable GFP (mito-paGFP) through the mitochondrial network over time offers a quantifiable index of mitochondrial fission/fusion dynamics. Thus, “dAKAP-high” MCF7 cells were co-transfected with photoactivatable mito-paGFP and photostable mito-dsRed mitochondrial markers (figs. 4.3a-c). Photoactivation within a 1 μm diameter region allowed selective visualization and tracking of mito-paGFP over a time course of 30 min (figs. 4.3a-c, lower panels). Excitation of mito-dsRed over the same time course allowed visualization of the entire mitochondrial network (figs. 4.3a-c; upper panels). In control cells, mito-paGFP rapidly diffused out of the region of activation, while in dAKAP1 depleted cells, activated mito-paGFP remained largely constrained within the region of activation (figs. 4.3a & b, e & f). Furthermore, rescue upon expression of siRNA-resistant SNAP-tagged murine dAKAP1 rescue construct restored the free diffusion of the photoactivated mito-paGFP into the mitochondrial network (figs. 4.3c, e & f, grey). Labeling with a cell permeable far-red SNAP-targeting fluorophore allowed detection of dAKAP1 in the rescued cells (fig. 4.3d).

The rate of dispersal of mito-paGFP outside the region of activation provided a condensed measure in which to quantify mitochondrial dynamics in these cells over 30 minutes (fig. 4.3f). Since activated mito-paGFP will instantaneously diffuse into any connected mitochondrion, the distribution of mito-paGFP immediately following photoactivation provided an independent means of assessing mitochondrial connectivity (fig. 4.3g). This analysis reveals that gene silencing of dAKAP1 corresponded with a more fragmented mitochondrial network (fig. 4.3g, yellow), whereas rescue reverses this effect (fig. 4.3g, grey). Collectively, the data in this section indicate that depletion of dAKAP1 enhances mitochondrial fragmentation by reducing the formation of elongated and interconnected mitochondrial networks.

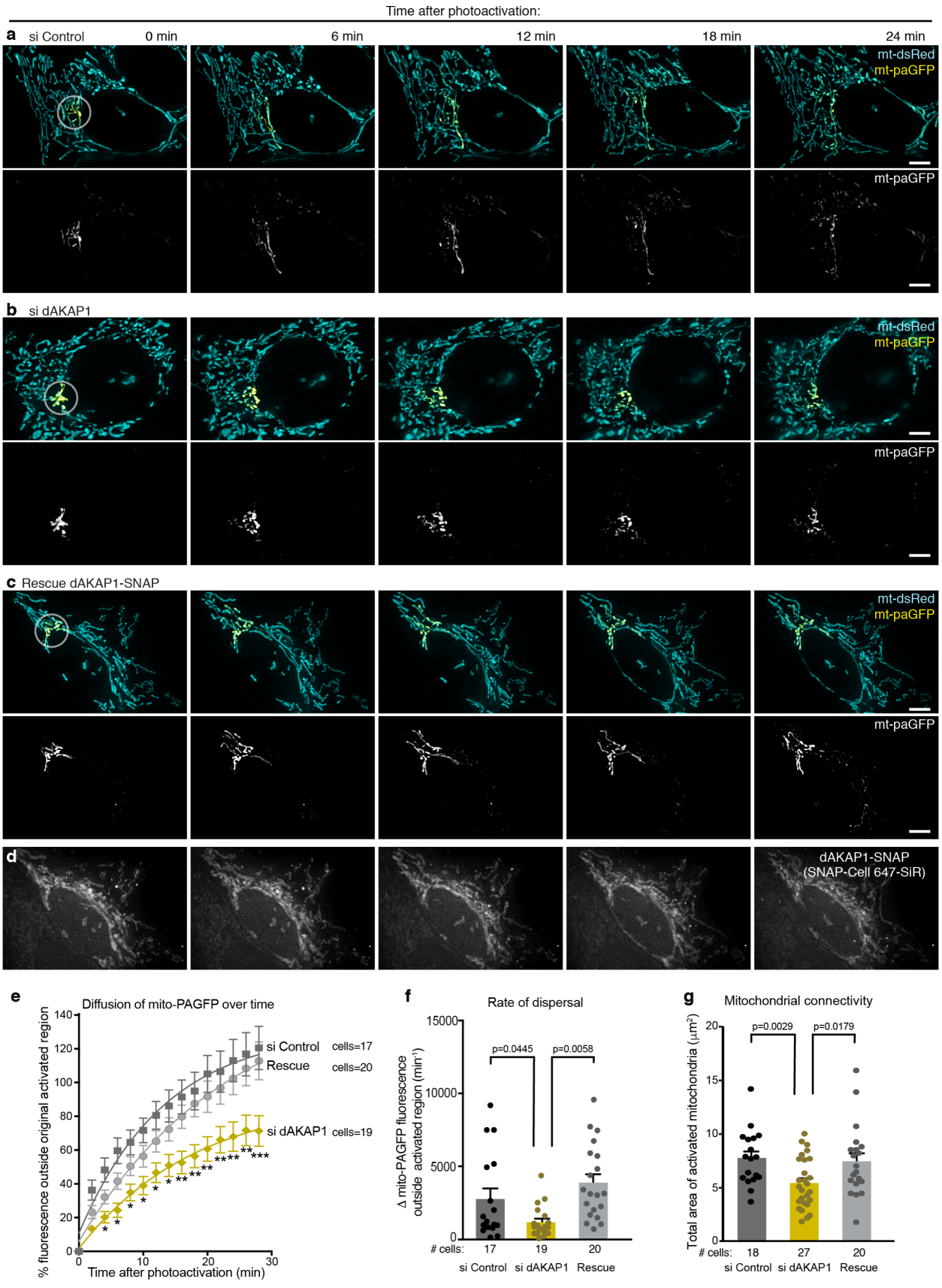
Time after photoactivation:
a si Control
0 min
6 min
12 min
18 min
24 min
mt-dsRed
mt-paGFP
mt-paGFP
b si dAKAP1
mt-dsRed
mt-paGFP
mt-paGFP
c Rescue dAKAP1-SNAP
mt-dsRed
mt-paGFP
mt-paGFP
d
dAKAP1-SNAP
(SNAP-Cell 647-SiR)
e
Diffusion of mito-PAGFP over time
% fluorescence outside original activated region
Time after photoactivation (min)
si Control cells=17
Rescue cells=20
si dAKAP1 cells=19
f
Rate of dispersal
Δ mito-PAGFP fluorescence outside activated region (min-1)
p=0.0445
p=0.0058
# cells: 17 19 20
si Control si dAKAP1 Rescue
g
Mitochondrial connectivity
Total area of activated mitochondria (μm2)
p=0.0029
p=0.0179
# cells: 18 27 20
si Control si dAKAP1 Rescue

Figure 4.3. Live-cell imaging analyses of mitochondrial dynamics. (a-c) Tracking of mitochondrially targeted photoactivatable GFP (paGFP; yellow) and whole cell detection of photostable mitochondrially targeted dsRed (teal) monitored mitochondrial dynamics over a time course of 30 min. Images were acquired of MCF7 cells treated with **(a)** si Control, **(b)** si dAKAP1, and **(c)** rescue upon expression of murine SNAP-tagged dAKAP1. Upper montage: composite images of both fluorescent channels. White circle denotes site of photoactivation. Lower montage: grey scale images of paGFP signal. **(d)** Detection of SNAP-tagged dAKAP1 upon conjugation with SNAP-cell 647-SiR fluorescent dye. Scale bars (5μm) are indicated. **(e)** Diffusion of fluorescent paGFP signal out of the region of activation was calculated. Amalgamated data for si Control (dark grey), si dAKAP1 (yellow), and rescued cells (grey). Numbers of cells in each analysis are indicated. Error bars represent s.e.m. Statistical significance was individually determined by two-tailed Student's t-test. **(f)** Rates of dispersal over the total time course and **(g)** degree of mitochondrial connectivity were calculated from acquired images. Number of cells used in each analysis is indicated below each column. Data was collected over n≥4 independent experiments. Error bars represent s.e.m. Statistical significance was determined by two-tailed Student's t-test. Welch's correction was used in (f) to account for uneven variances. Statistical significance convention: * is $p<0.05$; ** is $p<0.01$; *** is $p<0.001$.

4.2.3 Mitochondrial membrane potential is decreased when dAKAP1 is depleted

Since we established that endogenous dAKAP1 levels correlated with mitochondrial membrane potential in the representative breast cancer cell lines (section 3.2.2), it was important to determine if this was a direct effect related to changes in dAKAP1 levels. In "dAKAP1-high" MCF7 cells, dAKAP1 was depleted with either control or dAKAP1-targeting siRNA, as previously described. Mitochondrial membrane potential was assessed by determining the change in $\Delta\Psi_m$-dependent TMRM signal intensity (described in section 3.2.2) before and after complete membrane depolarization by FCCP (carbonyl cyanide-4-(trifluoromethoxy) phenylhydrazone), an uncoupling molecule that disrupts ATP synthesis[89]. A large magnitude of change after membrane depolarization is indicative of higher $\Delta\Psi_m$. Quantification confirmed that $\Delta\Psi_m$ was directly related to dAKAP1 expression levels, with a significant decrease in $\Delta\Psi_m$ observed after siRNA-mediated dAKAP1 depletion (fig 4.4a & b). This was shown independently in two experiments either using fluorescent microscopy (fig. 4.4a) or a fluorescent plate reader (fig. 4.4b).

4.2.4 Depletion of dAKAP1 decreases cell viability during nutrient deprivation

Our previous results suggested that dAKAP1 is required to drive nutrient deprivation-related mitochondrial elongation (section 4.2.1). This is relevant to *in vivo* tumor models because mitochondrial elongation is thought to be a generally protective mechanism by the cell in otherwise harsh nutrient deficient environments, such as that observed in the dense center of tumors[30,33]. Since overexpression of dAKAP1 was previously found to be protective in neurons[59,60], we hypothesized that conversely, depletion of this protein might sensitize breast cancer cells to cell death.

Therefore, we used siRNA in "dAKAP1-high" MCF7 cells (as described earlier in this section) to deplete dAKAP1 under either normal growth conditions or nutrient deprivation. To determine whether or not dAKAP1 expression and related changes in mitochondrial morphology influenced breast cancer cell viability, we used MTS (3-(4,5-dimethylthiazol-2-yl)-5-(3-carboxymethoxyphenyl)-2-(4-sulfophenyl)-2H-tetrazolium) to quantitatively measure viable cells over 48 hours[90]. Although no significant changes in viability were observed under normal growth conditions, the viability of dAKAP1 depleted cells dropped significantly after 48 hours of serum starvation (fig. 4.4c). Interestingly, CRISPR/Cas9 knockout of dAKAP1 proved lethal in all four representative breast cancer cell lines (data not shown), suggesting that some minimal level of this protein is required for normal cell growth and proliferation. These data support the hypothesis that dAKAP1 depletion sensitizes breast cancer cells to harsh environmental conditions, such as nutrient depravation, that are relevant to the tumor microenvironment. Furthermore, based on data described in previous sections, we postulate that these dAKAP1-related changes in viability are likely regulated through mitochondrial morphology and function.

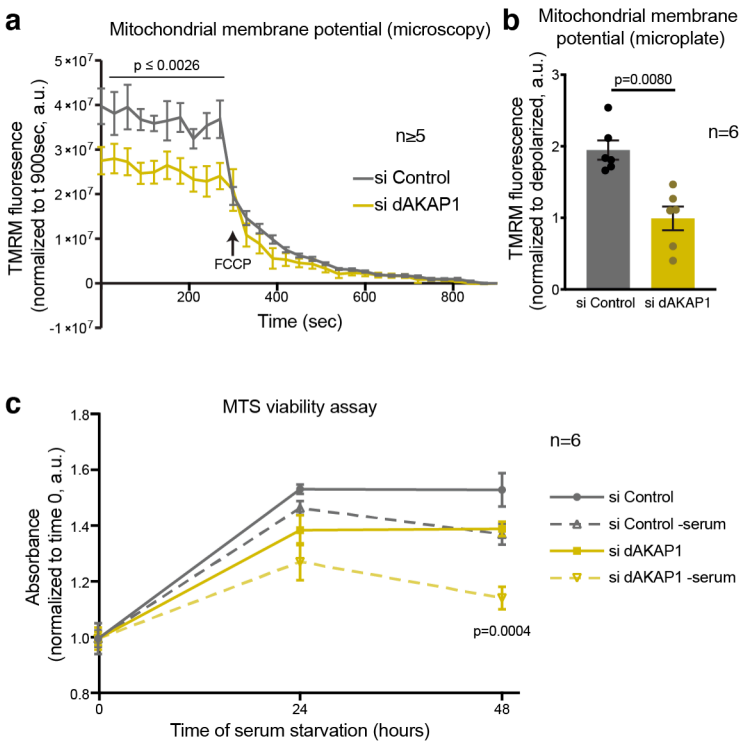

Figure 4.4. dAKAP1 depletion reduces membrane potential and decreases viability. (a) Images were acquired from "dAKAP1-high" MCF7 cells treated with control (dark grey) or dAKAP1-targeted (yellow) siRNA and loaded with $\Delta\Psi_m$-dependent fluorophore TMRM. After 300 seconds (5 mins), cells were completely depolarized with FCCP. TMRM fluorescence intensity was measured from individual cells over 900 seconds (15 mins). Data was collected over n≥5 independent experiments. Error bars represent s.e.m. Statistical significance was determined by two-tailed Student's t-test for each time point. **(b)** MCF7 cells were seeded onto a 96-well microplate and treated with control (dark grey) or dAKAP1-targeted (yellow) siRNA and loaded with $\Delta\Psi_m$-dependent fluorophore TMRM. Fluorescent signal intensity was read with and without FCCP depolarization. Data shown was normalized to post-FCCP treated intensity values. Data was collected over n=6 independent experiments; individual data points are shown. Error bars represent s.e.m. Statistical significance was determined by two-tailed Student's t-test. **(c)** MCF7 cells were treated with control (dark grey) or dAKAP1-targeted (yellow) siRNA grown in media with (solid lines) or without (dashed lines) serum. Viability was assessed via MTS assay over the course of 48 hours in respective growth conditions. Data was collected over n=6 independent experiments. Error bars represent s.e.m. Statistical significance was determined by two-tailed Student's t-test between serum-starved cells treated with si Control and those treated with si dAKAP1.

4.3 Conclusions

Experiments described in this chapter support the idea that dAKAP1 expression is generally protective in breast cancer cells. Live-cell imaging has allowed us to determine that dAKAP1 expression directly influences mitochondrial morphology through the phosphorylation of Drp1 at Ser637 (figs. 4.1 & 4.2). Furthermore, the photoactivation of a small portion of the mitochondrial network allowed us to visualize mitochondrial dynamics over time (fig. 4.3). While initial

differences in diffusion can be attributed solely to differences in morphology, the temporal aspect of these experiments additionally provides a quantitative measure of mitochondrial fusion. Since the diffusion of fluorophore into non-photoactivated mitochondria can only result from the fusion of mitochondrial membranes, dispersal rate is a measure of mitochondrial fusion independent of fission and morphology. Therefore, reduced dispersal rates observed with dAKAP1 depletion suggest that this protein may also have a corresponding role in mitochondrial fusion, in addition to its established role in fission. No previous role in mitochondrial fusion has been found for dAKAP1. A role in both of these processes would be substantial because it would poise dAKAP1 in a position to control both opposing aspects of mitochondrial dynamics.

Furthermore, we have established that dAKAP1 depletion prevents the mitochondrial elongation associated with serum starvation (fig. 4.2), resulting in decreased cellular viability (fig. 4.4). By depleting dAKAP1 expression in "dAKAP1-high" MCF7 cells, $\Delta\Psi_m$ was reduced (fig. 4.4), thereby linking dAKAP1 expression levels directly to changes in $\Delta\Psi_m$ and complementing the trends observed between breast cancer cell lines in Chapter 3. Similarly, dAKAP1 depletion caused reduced viability with serum starvation (fig. 4.4), which may be relevant to the tumor microenvironment. Taken together, results from this chapter suggest that dAKAP1 expression is generally protective to cells by supporting mitochondrial morphological responses to stress and mitochondrial membrane potential. Extrapolating these results to a more physiological situation, we postulate that this protective effect of dAKAP1 expression may translate to increased cancer cell viability in a dense, nutrient-restricted tumor. Therefore, reduced dAKAP1 levels may be related to increased efficacy of some treatments. However, since reductions of dAKAP1 expression were also associated with increased cell migration (Chapter 2), interpretation of these results may be complicated for the design of therapeutics.

Chapter 5:

Repression of cell motility and mitochondrial positioning by dAKAP1-anchored PKA

5.1 Introduction

The distribution of mitochondria within a cell can be indicative of localized energy demand. During the energetically taxing process of migration, mitochondria have been found to localize to the leading edge (LE) of migrating cells[54,55]. Smaller, more fragmented mitochondria have been found to facilitate this process in motile breast cancer cells[51,52]. Furthermore, PKA phosphorylation events at the LE of migrating cells are essential for motility[55]. Since dAKAP1 influences mitochondrial morphology and other PKA signaling events, we reasoned that expression of this anchoring protein could influence migration and invasion through either of these mechanisms. Moreover, dAKAP1-anchored PKA has also been shown to phosphorylate the oncoprotein Lfc, a microtubule-associated Rho guanine nucleotide exchange factor[66], suggesting that this protein may have a role in microtubule dynamics as well.

5.2 Results

5.2.1 Cell motility is inhibited by dAKAP1 expression in motile breast cancer cells

Tumor cell migration and the ability to invade other organs are defining features of metastatic cancer[91,92]. Fragmented mitochondrial networks and related Drp1 activity are reported to contribute to this motility in breast cancer cell lines[51]. Since dAKAP1-associated PKA prevents mitochondrial fragmentation via the phosphorylation of Drp1, we reasoned that this local signaling event could influence cell migration. In order to test this hypothesis, we investigated cell migration in motile “dAKAP1-low” MDAMB231 cells. Doxycycline-inducible lentiviral cell lines were generated to express either dAKAP1 or a PKA anchoring defective point mutant

(dAKAP1ΔPKA)[25] containing an N-terminal V5 epitope tag (fig. 5.1a). Transwell migration assays monitored cell movement through a permeable membrane toward chemoattractant media (figs. 5.1b & c). Migration of doxycycline-induced cells was normalized to their un-induced MDAMB231 counterparts that express low levels of endogenous dAKAP1 (fig. 5.1b & c). Doxycycline induction of wildtype dAKAP1 diminished MDAMB231 cell migration compared to un-induced control cells (fig. 5.1a, top panel, lane 2; fig. 5.1b, top right panel; & fig. 5.1c, dark grey squares). Interestingly, induction of the dAKAP1ΔPKA mutant mildly enhanced transwell migration (fig. 5.1a, top panel, lane 4; fig. 5.1b, bottom right panel; & fig. 5.1c, red triangles), suggesting a dominant negative effect. Similar results were obtained when these experiments were repeated using a transwell invasion assay to measure migration through a 3D matrix (Matrigel) toward chemoattractant media (figs. 5.1d & e). Two important pieces of information can be gleaned from these experiments: (1) conversion of the “dAKAP1-low” cell line MDAMB231 to “dAKAP-high” expressing cells blocks migration and (2) dAKAP1-anchored PKA is necessary for this process.

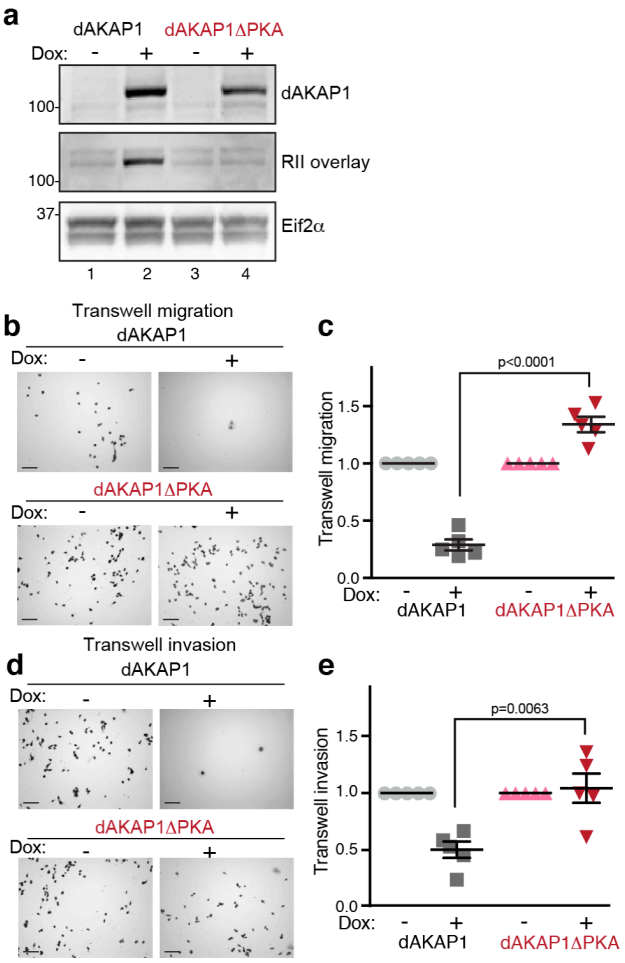

Figure 5.1. dAKAP1-anchored PKA represses cell motility. MDAMB231 cells were generated with either a doxycycline-inducible dAKAP1 or a PKA anchoring deficient mutant dAKAP1ΔPKA. **(a)** Immunoblot detection of V5-tagged dAKAP1 (top), PKA anchoring assessed by RII overlay (middle)[93], Eif2α loading control (bottom). **(b)** & **(c)** Transwell migration monitors cell movement across a porous membrane. **(b)** Representative images of crystal violet stained migrating cells under each experimental condition. Scale bars (100μm) are indicated. Experimental conditions indicated. **(c)** Amalgamated data (n=5 independent experiments) normalized to either un-induced "dAKAP1-low" wildtype dAKAP1 MDAMB231 cells (grey circles) or un-induced "dAKAP1-low" dAKAP1ΔPKA mutant MDAMB231 cells (pink triangles) in each experiment. Transwell migration of cells overexpressing dAKAP1 (dark grey squares) or dAKAP1ΔPKA (red triangles) is indicated. **(d)** & **(e)** Transwell invasion evaluates cell migration through a 3D Matrigel barrier. **(d)** Representative image of crystal violet stained invading cells under each experimental condition. Scale bars (100μm) are indicated. **(e)** Quantification of data (n=5 independent experiments) as defined above in (c). Error bars presented in (c) & (e) signify s.e.m. Statistical significance was determined by two-tailed Student's t-test.

5.2.2 Mitochondrial localization is inhibited by dAKAP1 expression in breast cancer cells

Imaging of migrating MDAMB231 cells loaded with Mitotracker Green FM into a scratch wound consolidated both of the above conclusions (figs. 5.1a-d). Migration velocity of individual un-induced control cells was calculated as 33.49 ± 2.76 μm/h over a time course of 18 hours (figs. 5.2a & d, grey column). Doxycycline induction of dAKAP1 expression diminished cell migration as evidenced by a reduced cell velocity of 22.40 ± 1.60 μm/h over the same time course (fig. 5.2b & d, dark grey column). Conversely, overexpression of the dAKAP1ΔPKA mutant restored rates of cell migration to control levels (34.86 ± 1.67 μm/h; fig. 5.2c & d, red column).

Anterior positioning of mitochondria toward the leading edge is associated with increased velocity and the directional persistence of migrating breast cancer cells[94]. Accordingly, we used time-lapse imaging to monitor the intracellular location of Mitotracker-stained mitochondria (figs. 5.2e-g). Mitochondrial localization indexes (MLI) were defined as the ratio of integrated fluorescent signal in front of the centroid (black dot) to the entire cell[94] (white line; figs. 5.2e-g, top panels). Line plots monitored the distribution of fluorescent mitochondria over the length of representative cells (figs. 5.2e-g, bottom panels). In control cells, the majority of mitochondria were positioned toward the anterior (leading edge) of cells (fig. 5.2e & h, grey column). As anticipated, induction of dAKAP1 reduced mitochondrial mass at the leading edge (anterior) (fig. 5.2f & h, dark grey column). This effect was lost in cells expressing dAKAP1ΔPKA, which largely resembled control cells (fig. 5.2g & h, red column). Thus we can conclude that local PKA signaling islands at the outer mitochondrial membrane suppress cell migration via changes in mitochondrial localization to the leading edge.

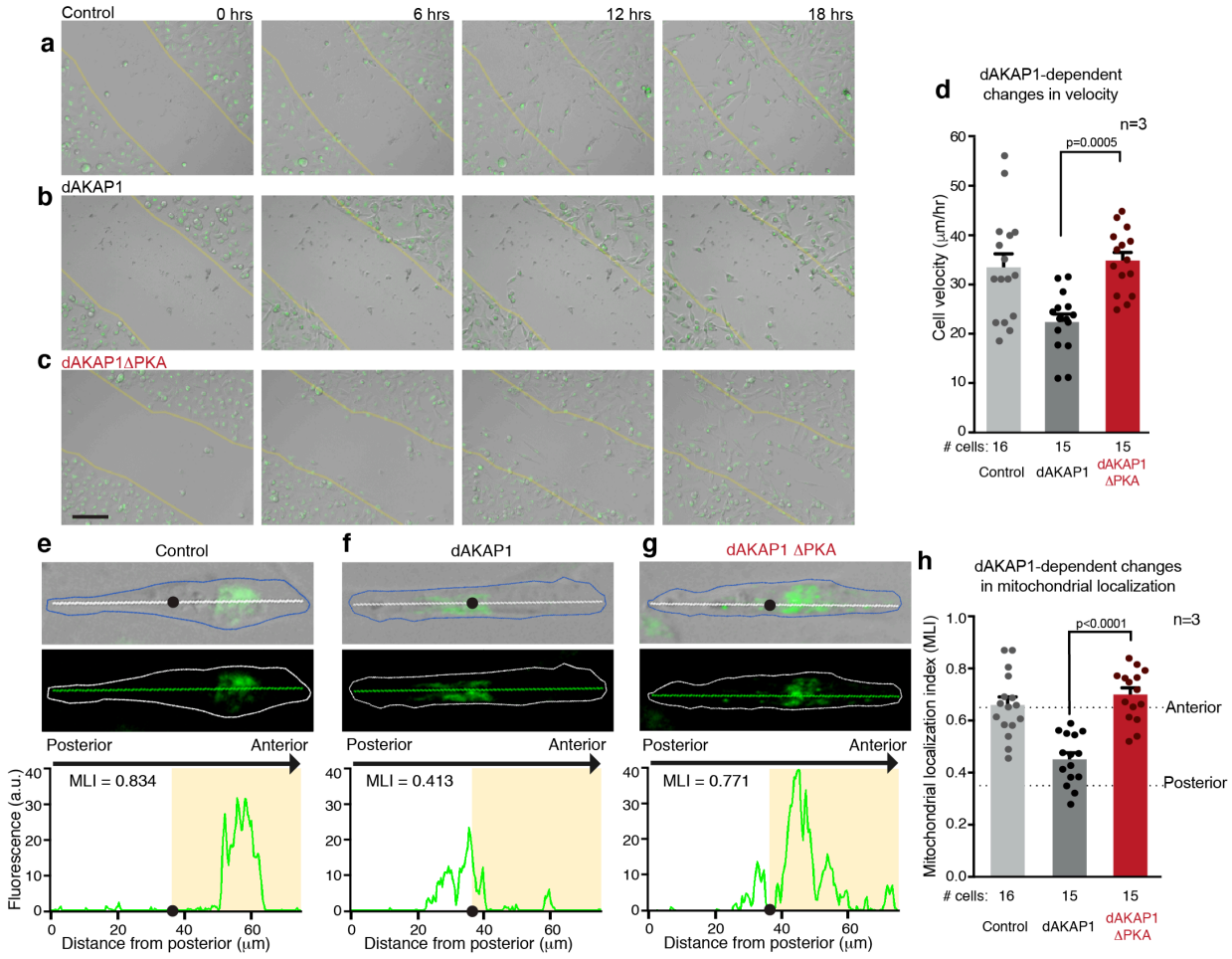

Figure 5.2. dAKAP1-anchored PKA suppresses mitochondrial positioning to the leading edge. **(a-d)** Migration of Mitotracker-loaded MDAMB231 cells into scratch wounds (yellow border) over a time course of 18 h. Montages of MDAMB231 **(a)** un-induced "dAKAP1-low" control cells and **(b)** cells overexpressing wildtype dAKAP1 or **(c)** dAKAP1ΔPKA mutant. **(d)** Migration velocities (μm/min) of control (grey) and cells overexpressing dAKAP1 (dark grey) or dAKAP1ΔPKA (red; n=3 independent experiments). Numbers of cells analyzed from three independent experiments are indicated. Scale bars (100μm) are indicated. **(e-h)** Fluorescent detection revealed the location of mitochondrial networks in migrating **(e)** control cells and cells **(f)** overexpressing dAKAP1 or **(g)** dAKAP1ΔPKA mutant. Representative images depict composite brightfield and Mitotracker signals (top), Mitotracker alone (middle), and posterior-anterior line plots (bottom) to reveal intracellular position of fluorescent mitochondria. Cell body is outlined. Lines to generate line plots are indicated (top, white & middle, green). Centroid (black circle) and anterior (yellow shaded regions) of migrating cells are indicated. Scale is defined by x-axis of line plot, 75μm. **(h)** Localization indexes[94] quantify the positioning of mitochondria in control (grey), wildtype dAKAP1 (dark grey), or dAKAP1ΔPKA (red) cells (n=3 independent experiments). Number of cells analyzed from three experiments is indicated. Error bars presented in (d) & (h) signify s.e.m. Statistical significance was determined by two-tailed Student's t-test.

5.2.3 Changes in dAKAP1 expression alter cytoskeletal phosphorylation events

In order to better understand the molecular events that underlay these changes in migration, phosphoproteomics was used to identify specific phosphoproteins that were strongly regulated with wildtype dAKAP1 overexpression. Using the same “dAKAP1-low” MDAMB231 cells with inducible dAKAP1 expression, both un-induced control and doxycycline-treated cells were analyzed via mass spectrometry. Of 12,040 total phosphosites identified, a small group of just 45 were found to be significantly regulated across 5 experimental replicates, of which only 11 represented a fold change of 2 or greater (table 5.1). This limited set of regulated phosphosites suggests that dAKAP1 expression does not ‘reprogram’ the cells, but rather controls very targeted processes to influence cell migration. Surprisingly, of the 11 phosphosites that were strongly regulated, dAKAP1 was the only mitochondrial-specific protein (table 5.1). Furthermore, many of the phosphoproteins identified had trafficking or cytoskeletal functions (table 5.2, red text), suggesting that dAKAP1 may alter migration by influencing cytoskeletal dynamics or organelle trafficking. Follow-up studies are necessary to validate these results and identify a mechanism.

Gene	Protein	Position	Intensity, un-induced (log2)	Intensity, +doxycycline (log2)	Fold change
SPTBN1	Spectrin beta chain, non-erythrocytic 1	2108	-6.163635667	2.6309432	8.79457887
AKAP1	A-kinase anchor protein 1, mitochondrial	533	-3.05965825	1.12670534	4.186363602
		150	0.679461	4.830806	4.151344967
		445	0.010671118	3.4458208	3.435149479
		429	1.304731	4.481053	3.176322174
ARHGAP5	Rho GTPase-activating protein 5	1195	0.9159112	-1.35369075	-2.269601727
GIPC1	PDZ domain-containing protein GIPC1	33	1.1462434	-1.1634135	-2.309657192
CEP170	Centrosomal protein of 170 kDa	261	2.2226962	0.0886093	-2.134086609
		258	1.980704	-0.4116821	-2.392386246
AFF4	AF4/FMR2 family member 4	706	1.6708584	-1.146984767	-2.817843119
MAP1B	Microtubule-associated protein 1B;MAP1B heavy chain;MAP1 light chain LC1	1785	0.83200268	-2.8334465	-3.665449142

Table 5.1. Phosphosites regulated with dAKAP1 overexpression in MDAMB231 cells. Seven phosphosites were identified as greater than 2-fold changed with phosphoproteomics. Phosphosites increased in phosphorylation with dAKAP1 expression are shaded in yellow, sites decreased are shaded in blue.

PANTHER GO-Slim Biological Process	Fold Enrichment
anatomical structure morphogenesis	21.32
protein targeting	**17.58**
nervous system development	9.57
cytoskeleton organization	**7.44**
cellular component morphogenesis	**7.11**
system development	6.65
cell differentiation	5.49
regulation of nucleobase-containing compound metabolic process	5.14
intracellular protein transport	**4.33**
protein transport	**4.08**
developmental process	4.01
transcription, DNA-dependent	2.95
organelle organization	**2.48**
nucleobase-containing compound metabolic process	2.15
PANTHER GO-Slim Molecular Function	
double-stranded DNA binding	81.24
acetyltransferase activity	39.55
microtubule binding	**27.83**
actin binding	**21.63**
nuclease activity	18.56
transferase activity, transferring acyl groups	16.16
cytoskeletal protein binding	**9.39**
hydrolase activity, acting on ester bonds	5.61
sequence-specific DNA binding transcription factor activity	3.73
nucleic acid binding	3.7
receptor binding	3.48
DNA binding	2.77
transferase activity	2.27
protein binding	**2.18**

Table 5.2. Gene ontology (GO) enrichment of phosphoproteins[95]. GO-slim term enrichment analysis by biological process and molecular function was performed on the seven phosphoproteins identified in Table 5.1. Biological processes and molecular functions relevant to mitochondrial function, trafficking, or cellular movement are highlighted in red. For each category, terms are organized by fold enrichment over a background proteome. Notably, none of the fold enrichments above were determined to be statistically significant ($p<0.05$), likely stemming from small sample size.

5.3 Conclusions

This chapter concludes our investigation into dAKAP1's role in metastatic breast cancer with observations in changes of cell motility. We found that induced expression of dAKAP1 in the normally "dAKAP1-low" cell line MDAMB231 reduced the motility of the cells both in migration and invasion assays (fig. 5.1). Furthermore, this decreased motility was linked to changes in mitochondrial positioning to the LE of migrating cells (fig. 5.2). These reductions in both motility and mitochondrial positioning are also dependent on the ability of dAKAP1 to anchor PKA (figs. 5.1 & 5.2). Combined, these data suggest that dAKAP1 expression reduces mitochondrial movement to the LE, where local energy demand is greater[55]. We hypothesize that this erroneous positioning of mitochondria contributes to decreased levels of motility.

Supplementing these findings, phosphoproteomics analysis of the same cells unveiled a limited number of phosphorylation changes when dAKAP1 is inducibly expressed (table 5.1). Robustly regulated sites included multiple proteins involved in cytoskeletal or trafficking functions (table 5.2), perhaps indicative of specific dAKAP1-induced changes in organelle trafficking. Contrary to our expectations, these results suggest that the observed decreases in migration are largely due to trafficking changes, rather than solely through dAKAP1-dependent changes in mitochondrial morphology (Chapter 4). Therefore, exploration of this new role in trafficking for dAKAP1 implores further investigation.

Taken together, our findings from Chapters 4 and 5 suggest that non-motile, "dAKAP1-high" cells have the molecular machinery in place to elongate mitochondrial networks as necessary, at the expense of decreased cellular migration and the ability to position mitochondria at the LE (fig. 5.3a, below). Conversely, the motile, "dAKAP1-low" cells lack the machinery to elongate mitochondria, perhaps at the expense of cell survival mechanisms. However, this expression

phenotype leads to more fragmented mitochondria and enhanced mitochondrial localization to the LE, with the end result of increased cellular migration (fig. 5.3b, below). We suggest a model in which dAKAP1 levels decrease as tumor cells progress towards metastasis to promote migration, and are subsequently increased when the metastatic site is seeded to promote viability (fig. 5.3c, below). This new model proposes that dAKAP1 controls various aspects of molecular signaling that are relevant to breast cancer metastasis, and may help establish rationale for new targets for therapeutic development.

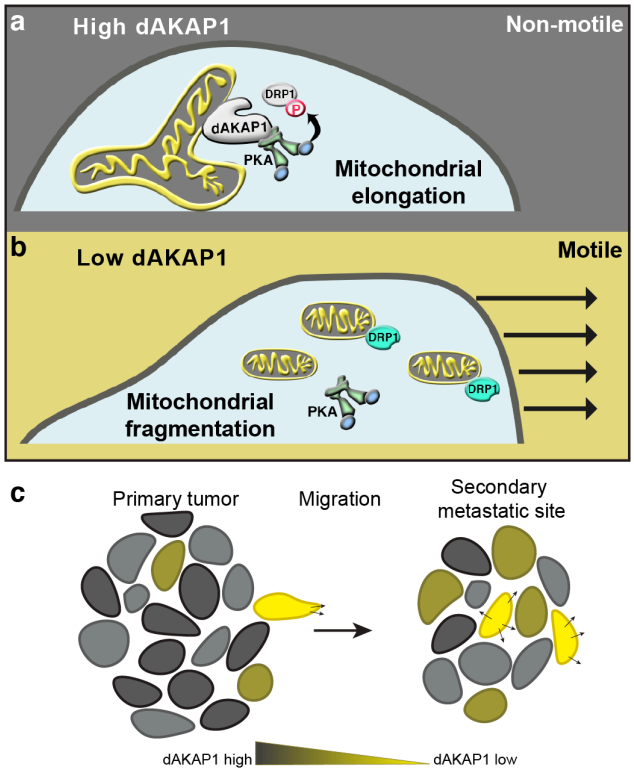

Figure 5.3. Schematic summarizing conclusions of this study. (a) High dAKAP1 expression favors non-motile breast cancer cells with elongated mitochondrial networks. **(b)** Low dAKAP1 levels result in fragmented mitochondria and enhanced cell motility. **(c)** Schematic of proposed model. dAKAP1 expression decreases as cells within the primary tumor progress towards metastasis. After seeding of the secondary site, dAKAP1 levels are increased to maintain viability, but to a lesser extent, perhaps sensitizing cells to migration and further metastasis.

Chapter 6:

Discussion

6.1 Changes in dAKAP1 expression in breast tumors

Consistent with published literature, we concur that breast cancer tumors contain high levels of dAKAP1, relative to surrounding stroma[21,73]. This is reflected in figure 2.3 where dAKAP1 is enriched in the tumor compartment. Results outlined in Chapter 4 suggest that high levels of dAKAP1 are protective and support mitochondrial function, particularly in conditions of nutrient deprivation relevant to the *in vivo* tumor environment[30]. Taken at surface level, these data suggest that dAKAP1 expression would support tumor cell health and viability, similar to what has been reported[17]. However, data presented in Chapters 2 and 5 suggest that the role for dAKAP1 is more complex when applied to metastatic progression. We propose a new dAKAP1-focused model of progression that distinguishes three phases of metastasis: (1) non-motile epithelial cells comprising primary tumor, (2) induction of a migratory phenotype in individual tumor cells, and (3) seeding of the metastatic site (fig. 5.3). Notably, these processes are analogous to that of EMT, migration, and subsequent MET (mesenchymal-to-epithelial transition) of migratory tumor cells[2]. An improvement over previous dAKAP1-related tumor models[17], our model accounts for tumor heterogeneity as well as changes in cellular expression patterns as tumor cells become migratory.

6.2 Key findings and implications

Through exploring various aspects of our proposed model, we have established that reduced expression of the mitochondrial PKA anchoring protein dAKAP1 correlates with tumor progression of breast cancers toward a malignant, migratory state. Analysis of both clinical

samples and cell lines show that dAKAP1 levels are inversely related to the expression of a mesenchymal profile. Therefore, we hypothesize that the migratory, mesenchymal-like cells responsible for tumor metastasis would have lower levels of dAKAP1 expression (figs. 2.1-2.3). Moreover, we have established that dAKAP1 expression levels are related to phenotypic variations of breast cancer cell lines including changes in metabolism, mitochondrial membrane potential, and invasive potential (figs. 3.1 & 3.3; fig. 4.4; figs. 5.1 & 5.2). Since previous work has implicated dAKAP1 in tumor growth and metabolism, we sought to further investigate these relationships[17].

After determining an association of dAKAP1 expression and various phenotypes, it was essential to identify signaling mechanisms behind these observed changes. Reduced dAKAP1 at the outer mitochondrial membrane decreased local signaling events that normally repress a migratory phenotype. This included loss of cAMP-responsive phosphorylation of Drp1 at Ser637 (figs. 4.1-4.2) and other signaling events that may be related to organelle trafficking (tables 5.1 & 5.2). Fragmentation of mitochondria occurs when PKA is displaced from dAKAP1[40,41]. This effect was exacerbated when dAKAP1 is depleted under the condition of serum starvation, when dAKAP1 normally facilitates mitochondrial elongation and promotes cell viability (figs. 4.2-4.4). We propose that subsequent trafficking of these smaller, more transportable mitochondria toward the leading edge may underlie cell motility and progression toward metastasis (fig. 5.3).

Intriguingly, the signaling events identified via phosphoproteomics in this study appear to occur mostly on cytoskeletal proteins, rather than mitochondrial, suggesting a novel role for dAKAP1 in cytoskeletal dynamics or trafficking during migration (tables 5.1 & 5.2). Based on this and results observed in figure 4.3, we speculate that changes in mitochondrial fusion could be related to mitochondrial trafficking and motility. Furthermore, dAKAP1 may also facilitate bi-directional control of these processes, as this anchoring protein simultaneously targets the

phosphatase PP1[42,63] as well as the cAMP-degrading enzyme PDE4a[64] to the OMM. Changes in cell motility may be further accentuated by the displacement of other dAKAP1-binding partners, including the microtubule-associated Rho guanine nucleotide exchange factor and oncoprotein Lfc[66]. These preliminary proteomic data suggest that dAKAP1 may serve as a nexus for the relay of signals between mitochondria and the microtubule network.

Since CRISPR-mediated knockout of dAKAP1 appeared to be lethal in breast cancer cell lines, but not unrelated lines such as HEK293 or MA10 (previously discussed in Chapter 4, data not shown), we postulate the existence of breast cancer-specific survival mechanisms that cause these cells rely on the expression of dAKAP1. This idea is consistent with observations that reduced levels of dAKAP1 sensitize cells to decreased viability as well as declines in important mitochondrial functions (fig. 4.4). Since dAKAP1 depletion has been implicated with a reduction in tumor growth[17], yet "dAKAP1-low" breast cancer cell lines are more migratory (fig. 3.1; figs. 5.1 & 5.2), we find further support for our model proposed in the beginning of this chapter.

6.3 A new model of dAKAP1-related changes in tumor development and progression

In this newly proposed model, we contemplate the involvement of dAKAP1 at each step (fig. 5.3). (1) Primary tumor epithelial cells express ample dAKAP1 to promote OXPHOS and facilitate mitochondrial morphological changes for protection from harsh environmental conditions. However, (2) when individual tumor cells adopt a migratory or mesenchymal phenotype, expression profiles are reprogrammed including a reduction in dAKAP1 levels (fig. 2.1 & 2.2). This reprogramming results in motile cells that favor glycolysis and contain low levels of dAKAP1. Migratory cells go on to invade other tissues of the body followed by (3) a shift back to an epithelial expression profile to form a secondary tumor including the return of dAKAP1 expression, albeit lower than that of the primary tumor (fig. 2.3; fig. 5.3). We speculate that this decreased metastatic site dAKAP1 expression may sensitize tumors to further metastasis as

tumors continue to grow. We propose that dAKAP1 is an important contributor to the progression of breast cancer metastasis, and that understanding the signaling events involved in this process will contribute to the development of targeted therapies aimed to reduce breast cancer metastasis.

6.4 Future directions

Given the implications with microtubule-related signaling suggested by the phosphoproteomics data, it will be imperative to follow up these results with biological experiments. Changes in mitochondrial trafficking could be experimentally determined in the doxycycline-inducible cells as well as with siRNA in MCF7 cells. Since this process can influence both cell migration and mitochondrial fusion, it could provide a mechanistic link between the changes observed in Chapters 4 and 5. Furthermore, investigating how dAKAP1-related signaling is related to cell viability would be critical to bring this study into a more clinical perspective. This could be accomplished with manipulation of dAKAP1 expression in breast cancer cell lines cultured in 3D to assess how dAKAP1 influences colony formation, outgrowth, mitochondrial dynamics, and cell viability with various cancer-related drug treatments. This model system could also be used to assess dAKAP1-related metabolic changes between non-motile and motile cells in a more physiological context than 2D culture. *In vivo* xenograft experiments could also be used to validate if “dAKAP1-low” cells are more capable of forming metastases than their “dAKAP1-high” counterparts, as we would predict based on the results of study. Bringing these ideas into a more clinically relevant model is critical to translate these findings to human metastatic breast cancer treatment.

Chapter 7:

Materials and Methods

7.1 Correlation and heat map generation

Cancer Cell Line Encyclopedia (CCLE) data[67]

RMA-normalized mRNA expression data were downloaded from the Broad Institute (https://portals.broadinstitute.org/ccle_legacy/home). Pearson's correlation was calculated between each AKAP with quantified mRNA expression values and individual mesenchymal markers[5] (36 total) in either breast cancer (fig. 2.1a-d) or any cancer etiology with >3 quantified cell lines (fig. 2.1 e & f) and represented in a heat map using Graphpad Prism 7 software (GraphPad software, La Jolla, CA).

Paired clinical sample RNA microarray, RNAseq, and proteomics data[70]

Microarray, RNAseq, and protein expression data were downloaded from the Broad Institute-associated browser (http://prot-shiny-vm.broadinstitute.org:3838/BC2016/). Pearson's correlation was calculated between dAKAP1 and expression of mesenchymal markers[5] (36 total) in individual samples and averaged across each of the 4 clinical subtypes defined in the study (fig. 2.2a & b)[70]. Resulting data was represented in a heat map using Graphpad Prism 7 software.

Clustering

Unsupervised hierarchical clustering was performed on mesenchymal genes (figs. 2.1b & f; figs. 2.2a & b, rows) using the Perseus software package (V1.6.1.3; Max Plank Institute of Biochemistry)[96] with the following settings: distance = Euclidean; linkage = average; process

with k-means enabled; number of clusters = 300; maximal number of iterations = 10; number of restarts = 1.

Determination of metabolic and invasive potential correlations

Data for oxygen consumption rate (OCR)/extracellular acidification rate (ECAR) was computationally determined from reported data[76] (figs. 3.1a & c, y-axis). Similarly, invasive potential was also computationally determined from published data[75] (figs. 3.1b & d, y-axis). These were compared to dAKAP1 protein expression values determined using iBAQ proteomics (figs. 3.1a & b, x-axis)[77] or mRNA expression (figs. 3.1c & d)[67]. Pearson's r was used to determine the linear relationship between OCR/ECAR and dAKAP1 expression, while Spearman's r was used for the non-linear variable of invasive potential. "Glycolytic" cells were defined as an OCR/ECAR ratio < 10. "Invasive" cell lines were defined as having an invasive potential of >250. See respective studies for relevant methods for determining OCR/ECAR[76] and invasive potential[75].

7.2 Cell & tissue biology

Antibodies

The following antibodies were used in this study for western blotting: AKAP149 (610720, BD Biosciences, 1:1,000), AKAP1 (HPA008691, Human Protein Atlas/Sigma Aldrich, 1:1,000), pDrp1 Ser637 (PA5-37534, Invitrogen, 1:1,000), total Drp1 (611739, BD Biosciences, 1:1,000), Eif2α (5324S, Cell Signaling Technologies, 1:1,000), V5 (R960CUS, Invitrogen, 1:5,000), and N-cadherin (13116S, Cell Signaling Technologies, 1:1,000), Snail (3879S, Cell Signaling Technologies, 1:500), E-cadherin (610181, BD Biosciences, 1:1,000), mouse and rabbit HRP-conjugated secondary antibodies (NA9310, NA9340, GE Life Sciences, 1:10,000).

The following antibodies and stains were used in this study for immunofluorescent imaging: AKAP1 (HPA008691, Human Protein Atlas, 1:500), DAPI (62248, LifeTechnologies, 1:1,000), Mitotracker Green FM (M7514, Invitrogen, 50nM), SNAP-cell 647-SiR (S9102S, New England BioLabs, 30nM). Secondary antibodies: donkey anti-rabbit AlexaFluor488 (A-21206, Invitrogen, 1:500) and donkey anti-rabbit AlexaFluor555 (A-31572, Invitrogen, 1:500).

Plasmids

The human dAKAP1 ORF was purchased from OriGene (RC200506). The pLIX403 plasmid was a gift from David Root (Addgene plasmid #41395). Mito-paGFP was a gift from Richard Youle (Addgene plasmid #23348). Plasmid encoding mito-dsRed was a gift from the lab of Suzanne Hoppins (University of Washington).

Cell lines and culture

Breast cancer cell lines MDAMB231 (ATCC cat. HTB-26), BT474 (ATCC cat. HTB-20), and HS578T (ATCC cat. HTB-126) were purchased from ATCC. MCF7 cells were graciously provided by the lab of Judit Villén (University of Washington). Cell lines were grown in Dulbecco's modified Eagle's medium (DMEM; Gibco) supplemented with 10% fetal bovine serum (FBS; Gibco). Cell lines with stably incorporated dAKAP1 variants were grown in DMEM supplemented with 10% defined, tetracycline-low FBS (Hyclone) with 1μg/mL puromycin (Sigma) unless otherwise noted. All cell lines were maintained in a 5% CO2 incubator at 37°C.

Serum starvation and siRNA

siRNA knockdown was achieved in MCF7 cells with 50nM AKAP1 siGENOME SmartPool (pool of 4 siRNAs) or 50nM siGENOME non-targeting siRNA (M-011426-02 and D-001210-03 respectively, Dharmacon) transfected with Lipofectamine2000 (ThermoFisher) and incubated in

a 5% CO_2 incubator at 37°C for 24 hours. Transfection media was replaced with FBS-free DMEM media after 24 hours to achieve 48 hours of serum starvation prior to assay.

Cell line generation

Doxycycline-inducible cells were generated using lentiviral transduction to stably incorporate dAKAP1 variants in a pLIX403 backbone. Lentiviral particles were incubated with MDAMB231 cells (ATCC) for 24 hours. Cells were recovered in normal media for 24 hours before undergoing 4μg/mL puromycin selection for 48 hours. After selection, cells were dissociated using 0.25% trypsin-EDTA (Gibco) and 200 cells were evenly distributed into a 10cm^2 dish and incubated for 48-96 hours or until single-cell derived colonies were visible. Single-cell derived colonies were hand picked with a pipet tip and plated into single wells of a 96-well plate. Cells were expanded and tested for induction with 1μg/mL doxycycline for 72 hours. Cell lines with moderate and comparably induced expression of V5-tagged dAKAP1 were selected for use in this study.

Tissue sample lysis

Tumor samples from breast cancer patients were obtained (fig. 2.2c; patients A-C, Northwest BioSpecimens; appx. A-1) as flash-frozen tissue. Tissue was powdered in a mortar on dry ice and lysed in RIPA buffer (150mM NaCl, 1% triton X-100, 0.5% Na deoxycholate, 0.1% SDS, 50mM Tris pH 8.0) with protease and phosphatase inhibitors by vortexing and incubating on a rocker at 4°C for 30 minutes. Lysates were cleared at 10,000xg for 10 minutes at 4°C. Lysate in fig. 2.2c, patient D was obtained from OriGene (catalog no. 543487; appx. A-1) in modified RIPA buffer.

Cell lysis

For lysis of cultured cells to be used for immunoblot (figs. 2.2c, 3.2a, 4.2a, & 5.1a), cell lines were grown to desired confluence and rinsed once in cold PBS. Cold lysis buffer (20mM HEPES pH 7.4, 150mM NaCl, 1mM EDTA, 0.5% Triton/NP-40 in water) with protease and phosphatase inhibitors was added to dish and gently rocked at 4°C for 20 minutes. Cell lysate was scraped into a chilled tube and cleared at 10,000xg for 10 minutes at 4°C.

Immunoblot analysis

BCA assay (Pierce) was used to determine protein concentrations and 15μg of protein per sample was loaded onto a Bolt 4-12% Bis-Tris gel (LifeTechnologies). Cleared lysate was boiled in 1X LDS loading buffer (ThermoFisher) for 10 minutes before loading. Proteins were transferred to nitrocellulose membrane and blocked in either 5% milk or 5% BSA in TBST, as determined by the manufacturer of the relevant antibody. Primary antibodies were incubated at dilutions described above overnight at 4°C. Blots were thoroughly washed in TBST before incubation in 1:10,000 secondary antibody for 1 hour at room temperature. Blots were washed again in TBST before imaging on an iBright FL1000 (ThermoFisher) with SuperSignal Dura ECL reagent (ThermoFisher). Densitometry for blot quantification was done using ImageJ software (NIH; http://rsb.info.nih.gov/ij).

Cell viability assay (MTS)

Cell viability was quantified with dAKAP1-depletion and nutrient deprivation (fig. 4.4c) using the MTS assay[90] (Promega, G3580). Cells were plated in 12 replicate wells in 100μL media in a 96-well plate and treated with siRNA, as described above. At 24 hours post-transfection, all wells were rinsed once in serum-free media before incubation in fresh, warm media with or without serum. At time = 0 hours of serum starvation, 20μL MTS reagent was added to one-third of the

replicates for each condition (4 wells each). MTS assay was repeated at time = 24 and 48 hours after serum starvation. For each timepoint, blank wells containing media only were included for background subtraction. Absorbance was read at 490nm for all relevant wells. Quantification represents background-subtracted absorbance normalized to time = 0 hours.

Transwell migration and invasion

MDAMB231 cells generated (described in 7.2, above) were induced to express dAKAP1 with 1μg/mL doxycycline treatment for 72 hours. Transwell assays (figs. 5.1b-e) were performed by dissociating treated cell lines in 1mM EDTA in PBS for 5 minutes at 37°C. Cells were agitated, fully resuspended in serum free media, and counted. A total of $1.0x10^5$ cells were seeded onto the upper chamber of the transwell. Transwells with an 8.0μm pore size were used uncoated for migration (Corning, 07-200-150) or matrigel-coated for invasion (Corning BioCoat, 354480). For matrigel invasion assays, matrigel-coated transwells were rehydrated in serum-free media at 37°C 5% CO_2 for 2 hours prior to seeding. Whole serum media (10% FBS in DMEM) was used as the chemoattractant in the bottom chamber. Migration assays were incubated at 37°C 5% CO_2 for 18 hours, invasion assays were incubated for 20 hours. After incubation, both chamber and membrane were rinsed 2x in PBS, fixed in 70% ethanol for 10 minutes, and stained in 0.05% crystal violet (w/v in water) for 30 minutes. Membranes and chambers were rinsed well in PBS and total cells in the bottom chamber were counted. Representative images were acquired at 10X magnification with a DMI8 automated inverted microscope (Leica), an EL6000 component (light source, filter wheel, ultra fast shutter, Leica), and a CoolSnap HQ camera (Photometrics).

7.3 Fixed cell and tissue imaging

Staining and antigen retrieval

For determination of dAKAP1 expression in human breast tissue (fig. 2.3c) Tissue section microarray of 50 paired primary and metastatic breast tumors was obtained from US BioMax (Br10010e; appx. A-2) as formalin-fixed paraffin embedded samples. Sections were deparaffinated (Citrasolv; Thermo-Fisher), antigen retrieval was performed (R-Buffer A, Retriever 2100 pressure cooker; Electron Microscopy Sciences), and tissue sections were blocked in 10% (v/v) donkey serum with 5% (w/v) BSA in PBS for at least 1 hour before overnight incubation with relevant primary antibodies.

Imaging and analysis

Cells were imaged on a Keyence BZ-X710 microscope using relevant filter cubes for brightfield (no filter), DAPI (blue filter), and dAKAP1 staining (red filter). All images were acquired with the same magnification (100X, oil immersion), exposure time, and illumination intensity. Images were quantified and processed using ImageJ software (NIH; http://rsb.info.nih.gov/ij).

Quantification of mitochondrial tumor enrichment

A quality review of each pair of tissue samples was completed by blindly scoring representative images with a quality score of 0 (poor), 1 (intermediate), or 2 (excellent). All pairs containing at least one score of 0 were disregarded for quantification (5 pairs out of 50 were discarded; appx. A-2, last column). Tumor cells and tumor stroma were identified by nuclear staining and tissue morphology (figs. 2.3a, b, d, e). Fluorescence intensity of dAKAP1 staining was measured as the average of three equivalent rectangles in regions of tumor cells and tumor stromal cells (figs. 2.3c & f). Values were normalized to DAPI staining to account for differences in cell density. A tumor enrichment ratio was calculated as a ratio of background-corrected DAPI-normalized dAKAP1 fluorescence intensity in tumor cells to that of stromal cells. Ratios ≥2.5

were considered “strong” staining, 2.5>ratios>1.5 were “intermediate,” and ratios ≤1.5 were scored as “weak” staining (figs. 2.3g & h).

Staining of breast cancer cell lines

To determine the distribution and relative expression of dAKAP1 within the breast cancer cell lines used in this study (fig. 3.2c), cells were grown to ~50% confluence. Cells were briefly rinsed with PBS and fixed in 4% paraformaldehyde for 10 minutes. Cells were permeabilized in 0.1% triton-X for 10 minutes, before blocking (PBS with 10% donkey serum, 0.1% triton-X, 1% BSA) for 1 hour to overnight at 4°C. Cells were stained with dAKAP1 and relevant antibodies (dilutions in section 7.2, above) in working buffer (PBS with 1% donkey serum, 0.1% triton-X, 1% BSA) and incubated overnight at 4°C. Relevant secondary antibodies (section 7.2, above) were incubated 1:500 in working buffer for 1 hour, washed in PBS, and stained with DAPI (LifeTechnologies, 62248) for 15 minutes. Coverslips were rinsed once in water and mounted in ProLong mounting media (ThermoFisher, P36965).

Cells were imaged on a Keyence BZ-X710 microscope using relevant filter cubes for DAPI and dAKAP1 staining. All images were acquired with the same magnification (100X, oil immersion), exposure time, and illumination intensities. Images were processed using ImageJ software (NIH; http://rsb.info.nih.gov/ij).

7.4 Live-cell imaging

Mitochondrial membrane potential of cell lines

For determination of $\Delta\Psi_m$ in breast cancer cell lines (fig. 3.3), cells were grown in media containing 10% FBS in a 5% CO_2 incubator at 37°C. On the day of imaging, media was aspirated and replaced with media containing 40nM TMRM (ThermoFisher, T668) and 50nM Mitotracker Green FM (Invitrogen, M7514), and incubated for 45 minutes at 37°C. Cells were

rinsed twice in PBS and further incubated in media containing NucBlue Hoescht 33342 stain (Invitrogen, R37605, 1 drop/mL) for 15 minutes at 37°C. Media was aspirated and replaced with Fluorobrite DMEM +10% FBS.

Cells were imaged on a GE Deltavision OMX SR microscope. After loading (above), cells were placed in a humidified chamber with 5% CO_2 at 37°C and imaged using a 60X oil immersion objective (Olympus). Nuclei were excited with a 405nm laser at 15%T for 100ms and captured at 435nm. Mitotracker FM was excited with a 488nm laser at 30%T for 150ms and captured at 528nm. TMRM was excited with a 568nm laser at 5%T for 50ms and captured at 609nm. All images were acquired with the same settings. Images were quantified by averaging three representative equivalent rectangles in each cell with each treatment condition. Images were processed using ImageJ software (NIH; http://rsb.info.nih.gov/ij).

Mitochondrial membrane potential of dAKAP1-depleted MCF7s

For determination of $\Delta\Psi_m$ in dAKAP1-depleted MCF7 cells (figs. 4.4a & b), siRNA knockdown was achieved in MCF7 cells with either 50nM AKAP1 targeting siRNA or 50nM non-targeting siRNA and transfected with Lipofectamine2000 as described in section 7.2). Transfection media was replaced with 10% FBS DMEM media after 24 hours to achieve a total of 48 hours of serum starvation prior to assay. Cells were loaded with 40nM TMRM for 45 minutes, as described above.

For microscopy analysis (fig. 4.4a) of $\Delta\Psi_m$, images were acquired every 30 seconds for 15 minutes. At time = 5 minutes, 25uM FCCP was added to the media. Membrane potentials were determined by measuring fluorescent intensity in three rectangles per cell and averaged. Data was normalized to average depolarized membrane potential at 15 minutes. Images were

acquired using a 63X oil immersion objective with a DMI8 automated inverted microscope (Leica), an EL6000 component (light source, filter wheel, ultra fast shutter, Leica), and a CoolSnap HQ camera (Photometrics).

For microplate analysis (fig. 4.4b) of $\Delta\Psi_m$, cells were plated in six replicates. Cells were treated with siRNA and loaded with 40nM TMRM, as described above. For depolarized control, cells were treated with FCCP for 5 minutes after loading with TMRM. Media was aspirated off and replaced with whole Fluorobrite media. Fluorescence intensity of each well was measured with 530nm excitation and 590nm emission. Wells containing only media were used to determine background fluorescence. Quantification of $\Delta\Psi_m$ reflects background-subtracted fluorescence intensity normalized to FCCP depolarized wells.

Mitochondrial morphology

To determine mitochondrial morphology in dAKAP1-depleted MCF7s (figs. 4.2c-f), cells were plated onto 35mm poly-L-lysine (Sigma) coated no.1.5 glass-bottomed dishes (P35G-1.5-10-C, MatTek) and treated as described above for siRNA transfection with serum starvation. On the day of imaging, media was aspirated and replaced with media containing 50nM Mitotracker Green FM (Invitrogen, M7514) and incubated for 45 minutes. Cells were rinsed twice in PBS and incubated in media containing NucBlue Hoescht 33342 stain (Invitrogen, R37605, 1 drop/mL) for 15 minutes at 37°C. Media was aspirated and replaced with serum-free Fluorobrite DMEM. Cells were imaged on a GE Deltavision OMX SR microscope. After loading (above), cells were placed in a humidified chamber with 5% CO_2 at 37°C and imaged using a 60X oil immersion objective (Olympus). Nuclei were excited with a 405nm laser at 15%T for 100ms and captured at 435nm. Mitotracker FM was excited with a 488nm laser at 30%T for 150ms and captured at 528nm. All images were acquired with the same settings. Images were quantified

and processed using ImageJ software (NIH; http://rsb.info.nih.gov/ij). Mitochondrial morphology quantification in figures 4.2e & f were quantified using the "Mitochondrial Morphology" ImageJ plugin[97].

Mitochondrial photoactivation

For photoactivation experiments illustrated in figure 4.3, cells were co-transfected with siRNAs (see above) and plasmids encoding mito-paGFP, mito-dsRed, and murine-dAKAP1-SNAP (rescue cells) using Lipofectamine 2000 (ThermoFisher). Cells were incubated in transfection media for 24 hours at 37°C. Transfection media was removed and replaced with serum-free DMEM and incubated for an additional 48 hours. On the day of imaging, cells were removed from media and loaded with 30nM SNAP-cell 647-SiR and incubated at 37°C for 30 minutes to label dAKAP1-SNAP. After incubation, cells were rinsed three times in PBS followed by incubation in serum-free media for an additional 30 minutes. Media was replaced with warmed serum-free media and moved to a 5% CO_2 microscope chamber for imaging at 37°C.

Cells were imaged on a GE Deltavision OMX SR microscope and imaged using a 60X oil immersion objective (Olympus). Z-stacks were acquired over 2μm with steps every 0.5μm. Quantification was done on sum intensity z-projections, while representative images are displayed as max intensity z-projections. Mitochondrial-paGFP was photoactivated with a 405nm laser at 1%T for 2ms in a 1μm diameter spot. Activated mito-paGFP fluorescent signal was excited at 488nm and captured at 528nm. Mitochondrial-dsRed fluorescence was excited at 568nm and captured at 609nm. For dAKAP1-SNAP rescue cells, SNAP-cell SiR647 was excited at 640nm at 20%T for 30ms and captured at 683nm. Images were captured every 2 minutes, starting 2 minutes before activation (time = -2 minutes), for 30 minutes. Time 0 minutes

corresponds to the time point immediately following initial photoactivation. All images were acquired with the same settings.

Quantification of photoactivated mitochondria diffusion

To quantify the diffusion of fluorescence intensity outside of the activated region over time (figs. 4.3a-c, e), a polygon was drawn using ImageJ software to contain the entire cell, carefully excluding only the photoactivated region at time = 0 minutes, and integrated fluorescence intensity was measured. The excluded area was defined by connecting the outermost edges of the photoactivated mitochondrial region and varies dependent on the elongation and interconnection of the mitochondrial network. The diffusion of photoactivated fluorophore outside of the activated region was then calculated by subtracting background so that time = 0 minutes was equal to 0 for each time point and expressed as a percentage of the initial (time = 0 minutes) integrated fluorescence intensity within the activated region.

Rate of diffusion and mitochondrial connectivity

The rate of diffusion (fig. 4.3f) was calculated as the difference between the integrated fluorescent intensity outside of the activated region (quantification described above) at the final time point (t=28 minutes) from that at the time of activation (t=0 minutes) divided by time (28 minutes). Mitochondrial connectivity (fig. 4.3g) was determined as the area of activated region determined by binary mask (isodata ImageJ algorithm) of image at time of activation (t=0min). Images were quantified and processed using ImageJ software (NIH; http://rsb.info.nih.gov/ij).

Migration into wounds

For the quantification of cellular migration into wounds (fig. 5.2), relevant cell lines were seeded into 4-chamber glass bottomed, TC-treated dishes (Gibco, AdvanceTC) to achieve a confluent monolayer at the time of the assay. Cells were loaded with 50nM Mitotracker Green FM for 1

hour in a 37°C 5% CO_2 incubator. Cells were rinsed once in PBS and incubated in CO_2-buffered Fluorobrite (Gibco) media + 10% FBS for 30 minutes. Monolayers were gently scratched with a P10 pipet tip to induce a wound healing response, then immediately rinsed twice in PBS. Cells were returned to CO_2-buffered Fluorobrite media + 10% FBS in a humidified 37°C 5% CO_2 imaging chamber on a Keyence BZ-X710 using a 20X magnification objective. Cells were imaged every 10 minutes for 18 hours.

Quantification of mitochondrial migration and MLI

Velocity of migration was quantified by analyzing the migration of individual cells into the wound region (fig. 5.2d). Distance traveled at the leading edge was determined for a minimum of 15 cells over the span of 1 hour (6 images) under each condition, over the course of three independent experiments. Mitochondrial localization index (MLI) of individual cells migrating into the wound region was calculated as described[94], with slight modification to avoid photosensitivity observed when nuclei were imaged. This modification involved setting the cell centroid as the centroid of the line drawn from the trailing edge to the leading edge (figs. 5.2e-g, black dots), rather than the nucleus. MLI was calculated as a ratio of integrated density anterior of the centroid over that of the total line (thus MLI ≤1). The MLI of each migrating cell was measured repeatedly in a sequence of 5 time steps and averaged (fig. 5.2h). Indexes less than 0.35 were scored as “posterior” localization, greater than 0.65 were scored as “anterior” localization, and MLIs between these values were considered generally mislocalized, as previously described[94].

Patient-derived samples

Breast cancer tumor samples (fig. 2.2c, patients A-C) were obtained from Northwest BioSpecimens following guidelines of ‘non-human research’ study procedures with guidance from the Human Subjects Division at the University of Washington. Remaining samples were

obtained through commercial sources such that patient privacy was protected by the manufacturer (tumor lysate, OriGene, fig. 2.2c, patient D; tissue slice microarray, US BioMax, figs. 2.3).

Statistical analysis

All data are presented as the mean ± s.e.m. unless otherwise indicated. Sample size (n) indicates the number of independent experiments represented in amalgamated data; total cell numbers used in these experiments are indicated. Statistical significance was typically determined using unpaired, two-tailed Student's t-test. When variances were determined to be significantly different, Welch's correction was applied. Significance between >2 samples (fig. 3.2b & fig. 3.3d) was calculated using one-way ANOVA, with Tukey's test for multiple comparisons applied. In all cases, significance was determined as $p \leq 0.05$. All analysis was performed in Graphpad Prism 7 software.

7.5 Phosphoproteomics of doxycycline-inducible MDAMB231 cell lines

Preparation phosphopeptides for global MS-phosphoproteomics analysis

(performed by Martin Golkowski, Shao-En Ong lab)

MDAMB231 cells generated to express wildtype dAKAP1 (described in 7.2, above) were induced with or without 1μg/mL doxycycline treatment for 72 hours. Adherent cells on a 25 cm dish were rinsed twice with ice cold PBS, excess PBS was removed thoroughly, and cells were harvested in 750 μL of 6 M aq. guanidine hydrochloride (Gdn*HCl) containing 100 mM Tris, 5 mM tris(2-carboxyethyl)phosphine hydrochloride (TCEP*HCl) and 10 mM chloroacetamide (CAM), pH 8.5, using a cell scraper. Cell lysates were pipetted into 1.5 mL microtubes, vortexed briefly and then heated to 95°C for 5 min[98]. Samples were then sonicated in a Qsonica cup sonicator (Newton, CT) at 100 W for 10 min (30 seconds on, 30 seconds off) on ice. Protein

content was measured using the Pierce 660 nm assay reagent (Thermo Fisher Scientific, Waltham, MA). Aliquots of 300 µg of protein were pipetted into a new tube and diluted 2-fold with 100 mM triethylammonium bicarbonate (TEAB) pH = 8.5. 3 µg of sequencing-grade endoproteinase Lys-C (Wako, Richmond, VA) were added (1:100 ratio) and the mixture agitated on a thermomixer at 1400 rpm at 37°C for 2 h. The mixture was diluted another 2-fold with 100 mM TEAB pH = 8.5 and 3 µg of trypsin were added. The mixture was agitated on a thermomixer at 1400 rpm at 37°C for overnight, acidified with formic acid (1% final), and cleared by centrifugation for 10 min at RT and 14,000 rcf. Peptides were extracted from the supernatant using Oasis HLB 1cc (10 mg) extraction cartridges (Waters, Milford, MA). Cartridges were activated by passing through 200 µL of methanol followed by 200 µL 80% aq. ACN containing 0.1% TFA, equilibrated with 400 µL 1% aq. formic acid. Peptides were loaded and then washed with 400 µL 1% aq. formic acid. Peptides were eluted with 300 µL 80% aq. ACN containing 0.1% TFA and directly subjected to the published batch IMAC phosphopeptide enrichment protocol with the following minor modifications[99]. 20 µL of a 50% IMAC bead slurry composed of 1/3 commercial PHOS-select iron affinity gel (Sigma Aldrich), 1/3 in-house made Fe^{3+}-NTA superflow agarose and 1/3 in-house made Ga^{3+}-NTA superflow agarose were used for phosphopeptide enrichment[100]. The IMAC slurry was washed three times with 10 bed volumes of 80% aq. ACN containing 0.1% TFA and phosphopeptide enrichment was performed in the same buffer. Phosphopeptides were desalted using C18 StageTips according to the published protocol with the following minor modifications[101]. After activation with 50 µL methanol and 50 µL 80% aq. ACN containing 0.1% TFA the StageTips were equilibrated with 50 µL 1% aq. formic acid. Then the peptides that were reconstituted in 50 µL 1% aq. formic acid were loaded and washed with 50 µL 1% aq. formic acid. The use of 1% formic acid instead of 5% aq. ACN containing 0.1% TFA prevents the loss of highly hydrophilic phosphopeptides.

nanoLC-MS/MS phosphoproteomics analysis *(performed by MG)*

The LC-MS/MS analyses were performed on a Thermo Fisher Scientific Orbitrap Elite instrument (Waltham, MA) as described previously with the following minor modifications[102]. Peptide samples were separated on a Thermo-Dionex RSLCNano UHPLC instrument (Sunnyvale, CA) using 20 cm long fused silica capillary columns (100 μm ID) packed with 3 μm 120 Å reversed phase C18 beads (Dr. Maisch, Ammerbuch, DE). For phosphopeptide samples the LC gradient was 120 min long with 3−30% B at 300 nL/min. LC solvent A was 0.1% aq. acetic acid and LC solvent B was 0.1% acetic acid, 99.9% acetonitrile. Data-dependent analysis was applied using Top15 selection with CID fragmentation.

Computation of MS raw files *(performed by MG)*

Raw files were analyzed by MaxQuant/Andromeda[103] version 1.5.2.8 using protein, peptide and site FDRs of 0.01 and a score minimum of 40 for modified peptides, 0 for unmodified peptides; delta score minimum of 17 for modified peptides, 0 for unmodified peptides. MS/MS spectra were searched against the UniProt human database (updated July 22nd, 2015). MaxQuant search parameters: Variable modifications included Oxidation (M) and Phospho (S/T/Y). Carbamidomethyl (C) was a fixed modification. Max. missed cleavages was 2, enzyme was Trypsin/P and max. charge was 7. The MaxQuant “match between runs” feature was enabled. The initial search tolerance for FTMS scans was 20 ppm and 0.5 Da for ITMS MS/MS scans.

Data Processing and statistical analysis *(performed by MG)*

MaxQuant raw data was processed, statistically analyzed and clustered using the Perseus software package v1.5.6.0[96]. Human gene ontology (GO) terms (GOBP, GOCC and GOMF) were loaded from the Perseus Annotations file downloaded on the 01.08.2017. Expression columns (phosphopeptide MS intensities) were log2 transformed and normalized by subtracting the median log2 expression value of each column from each expression value of the

corresponding column. Potential contaminant, reverse hits and proteins only identified by site were removed. Reproducibility was analyzed by column correlation (Pearson's r) and replicates that showed a variation of >0.25 in the r value compared to the mean r-values of all replicates of the same experiment were removed as outliers. Significant differences in phosphopeptide expression between experiments were quantified with a two-tailed two sample t-test with unequal variances and Benjamini-Hochberg correction for multiple comparisons was applied (FDR = 0.05).

Gene ontology enrichment analysis of results

The Gene Ontology (GO) enrichment analysis tool[95] was used online at: http://pantherdb.org. GO-slim term enrichment analysis by biological process and molecular function was performed on the seven phosphoproteins identified in Table 5.1.

Appendix A:

Description of patient samples

1. Supplementary to figure 2.2c. Patient samples for immunoblot.

Patient	Source	SKU	ER	PR	HER	Tumor Grade
A	NW BioS	185667	+	+	-	II
B	NW BioS	151767	+	+	-	III
C	NW BioS	186239	-	-	-	III
D	Origene	543487	+	+	-	II

2. Supplementary to figure 2.3. Tissue section microarray.

Pos.	Age	Sex	Anatomic Site	Pathology Diagnosis	TNM	Grade	Tissue ID	ER	PR	HER 2	Quality Score
A1	42	F	Breast	IDC	T2N2 M0	1	Fmg020772	-	*	0	2
A2	58	F	Breast	IDC	T2N1 M0	1	Fmg010766	+++	*	0	2
A3	40	F	Breast	IDC	T2N2 M0	2	Fmg020433	-	*	1+	2
A4	80	F	Breast	IDC	T2N2 M0	2	Fmg010939	-	*	2+	2
A5	78	F	Breast	IDC	T2N1 M0	1	Fmg020861	++	*	0	2
A6	39	F	Breast	IDC	T3N1 M0	1	Fmg021019	-	*	0	2
A7	48	F	Breast	IDC	T3N1 M0	1	Fmg020962	-	*	2+	1
A8	44	F	Breast	IDC	T2N2 M0	2	Fmg060243	-	*	2+	2
A9	52	F	Breast	IDC	T2N1 M0	-	Fmg020652	++	*	2+	2

A10	48	F	Breast	IDC	T2N1 M0	2	Fmg020768	-	*	0	2
B1	52	F	Breast	IDC	T2N1 M0	2	Fmg100132	-	-	3+	0
B2	48	F	Breast	IDC	T4N2 M0	2	Fmg060115	+++	-	0	2
B3	66	F	Breast	IDC	T1N1 M0	2	Fmg020534	-	-	1+	2
B4	42	F	Breast	IDC	T2N1 M0	1	Fmg020539	-	-	3+	2
B5	70	F	Breast	IDC	T2N1 M0	2	Fmg020578	-	-	2+	2
B6	56	F	Breast	IDC	T2N1 M0	2	Fmg020026	++	*	0	1
B7	44	F	Breast	IDC	T2N1 M0	2	Fmg050440	-	*	3+	2
B8	45	F	Breast	IDC	T2N1 M0	2	Fmg100181	-	*	2+	1
B9	53	F	Breast	IDC	T2N1 M0	2	Fmg020743	-	*	2+	2
B10	49	F	Breast	IDC	T2N1 M0	1	Fmg020530	-	-	2+	2
C1	53	F	Breast	IDC	T2N1 M0	2	Fmg050513	+++	++	0	2
C2	61	F	Breast	IDC	T2N1 M0	2	Fmg030088	-	-	0	1
C3	50	F	Breast	IDC	T3N1 M0	2	Fmg050365	+	-	0	2
C4	31	F	Breast	IDC	T3N1 M0	2	Fmg050134	+	-	0	2
C5	58	F	Breast	IDC	T2N2 M0	2	Fmg021040	++	-	0	2
C6	75	F	Breast	IDC	T3N1 M0	2	Fmg050236	-	-	0	2
C7	59	F	Breast	IDC	T2N2 M0	2	Fmg010537	+	-	3+	2
C8	52	F	Breast	IDC	T2N2 M0	2	Fmg010536	+++	-	2+	2
C9	28	F	Breast	IDC	T2N2 M0	2	Fmg020572	++	++	0	2
C10	55	F	Breast	IDC	T2N2 M0	2	Fmg100167	-	-	2+	2
D1	52	F	Breast	IDC	T4N1 M0	-	Fmg030226	*	*	*	2

D2	46	F	Breast	IDC	T3N2 M0	2	Fmg020771	-	-	2+	2
D3	51	F	Breast	IDC	T4N0 M0	2	Fmg020326	++	++	0	2
D4	35	F	Breast	IDC	T4N2 M0	2	Fmg050844	++	+++	0	2
D5	48	F	Breast	IDC	T3N1 M0	3	Fmg020869	-	-	0	2
D6	42	F	Breast	IDC	T2N2 M0	2	Fmg010821	+	+	0	2
D7	49	F	Breast	IDC	T3N1 M0	-	Fmg050520	++	-	2+	2
D8	49	F	Breast	IDC	T3N2 M0	2	Fmg010541	-	-	0	2
D9	50	F	Breast	IDC	T4N2 M0	3	Fmg040683	+++	++	0	2
D10	52	F	Breast	IDC	T2N1 M0	3	Fmg060191	-	-	0	2
E1	54	F	Breast	IDC	T2N2 M0	3	Fmg100282	-	-	0	2
E2	39	F	Breast	IDC	T4N2 M0	3	Fmg060154	-	-	0	2
E3	50	F	Breast	IDC	T2N1 M0	3	Fmg100164	-	-	0	2
E4	42	F	Breast	IDC	T2N1 M0	3	Fmg110138	+++	-	0	1
E5	33	F	Breast	IDC	T3N3 M0	3	Fmg021542	-	-	0	2
E6	48	F	Breast	IDC	T2N2 M0	2	Fmg110129	-	-	3+	2
E7	53	F	Breast	IDC	T4N2 M0	3	Fmg020963	-	-	0	2
E8	70	F	Breast	ILC	T2N2 M0	-	Fmg032386	++	-	2+	2
E9	72	F	Breast	ILC	T2N1 M0	-	Fmg050354	-	+	2+	1
E10	39	F	Breast	ILC	T2N1 M0	-	Fmg050785	-	-	0	1
F1	42	F	Lymph node	Met. of A1	-	-	Fmg020772	+	++	2+	2
F2	58	F	Lymph node	Met. of A2	-	-	Fmg010766	+++	+++	0	2
F3	40	F	Lymph node	Met. of A3	-	-	Fmg020433	-	-	1+	2

F4	80	F	Lymph node	Met. of A4	-	-	Fmg010939	-	-	3+	2
F5	78	F	Lymph node	Met. of A5	-	-	Fmg020861	+	+	0	2
F6	39	F	Lymph node	Met. of A6	-	-	Fmg021019	-	-	0	2
F7	48	F	Lymph node	Met. of A7	-	-	Fmg020962	-	-	0	0
F8	44	F	Lymph node	Met. of A8	-	-	Fmg060243	-	+	3+	2
F9	52	F	Lymph node	Met. of A9	-	-	Fmg020652	+++	-	0	2
F10	48	F	Lymph node	Met. of A10	-	-	Fmg020768	-	++	0	1
G1	52	F	Lymph node	Met. of B1	-	-	Fmg100132	-	-	3+	2
G2	48	F	Lymph node	Met. of B2	-	-	Fmg060115	+++	-	0	2
G3	66	F	Lymph node	Met. of B3	-	-	Fmg020534	++	++	0	2
G4	42	F	Lymph node	Met. of B4	-	-	Fmg020539	-	-	3+	2
G5	70	F	Lymph node	Met. of B5	-	-	Fmg020578	-	-	3+	2
G6	56	F	Lymph node	Met. of B6	-	-	Fmg020026	-	-	0	1
G7	44	F	Lymph node	Met. of B7	-	-	Fmg050440	-	-	3+	2
G8	45	F	Lymph node	Met. of B8	-	-	Fmg100181	-	-	3+	2
G9	53	F	Lymph node	Met. of B9	-	-	Fmg020743	-	-	2+	2
G10	49	F	Lymph node	Met. of B10	-	-	Fmg020530	-	-	1+	2
H1	53	F	Lymph node	Met. of C1	-	-	Fmg050513	+	-	1+	2
H2	61	F	Lymph node	Met. of C2	-	-	Fmg030088	-	-	0	2
H3	50	F	Lymph node	Met. of C3	-	-	Fmg050365	+++	+	0	1
H4	31	F	Lymph node	Met. of C4	-	-	Fmg050134	++	-	0	2
H5	58	F	Lymph node	Met. of C5	-	-	Fmg021040	++	-	0	2

H6	75	F	Lymph node	Met. of C6	-	-	Fmg050236	-	-	0	2
H7	59	F	Lymph node	Met. of C7	-	-	Fmg010537	++	-	1+	2
H8	52	F	Lymph node	Met. of C8	-	-	Fmg010536	+	-	2+	2
H9	28	F	Lymph node	Met. of C9	-	-	Fmg020572	++	++	0	2
H10	55	F	Lymph node	Met. of C10	-	-	Fmg100167	+	+++	0	2
I1	52	F	Lymph node	Met. of D1	-	-	Fmg030226	-	-	2+	2
I2	46	F	Lymph node	Met. of D2	-	-	Fmg020771	*	*	*	0
I3	51	F	Lymph node	Met. of D3	-	-	Fmg020326	+	+	0	2
I4	35	F	Lymph node	Met. of D4	-	-	Fmg050844	++	+++	0	2
I5	48	F	Lymph node	Met. of D5	-	-	Fmg020869	-	-	0	1
I6	42	F	Lymph node	Met. of D6	-	-	Fmg010821	*	*	0	0
I7	49	F	Lymph node	Met. of D7	-	-	Fmg050520	+	-	3+	2
I8	49	F	Lymph node	Met. of D8	-	-	Fmg010541	-	-	0	1
I9	50	F	Lymph node	Met. of D9	-	-	Fmg040683	+++	+	0	2
I10	52	F	Lymph node	Met. of D10	-	-	Fmg060191	-	-	0	2
J1	54	F	Lymph node	Met. of E1	-	-	Fmg100282	-	-	0	0
J2	39	F	Lymph node	Met. of E2	-	-	Fmg060154	-	-	0	2
J3	50	F	Lymph node	Met. of E3	-	-	Fmg100164	-	-	0	2
J4	42	F	Lymph node	Met. of E4	-	-	Fmg110138	+	-	0	1
J5	33	F	Lymph node	Met. of E5	-	-	Fmg021542	-	-	0	2
J6	48	F	Lymph node	Met. of E6	-	-	Fmg110129	-	-	3+	2
J7	53	F	Lymph node	Met. of E7	-	-	Fmg020963	-	-	0	2

J8	70	F	Lymph node	Met. of E8	-	-	Fmg032386	+++	+	3+	2
J9	72	F	Lymph node	Met. of E9	-	-	Fmg050354	++	++	2+	2
J10	39	F	Lymph node	Met. of E10	-	-	Fmg050785	-	-	0	2

Appendix B:

Un-cropped immunoblots

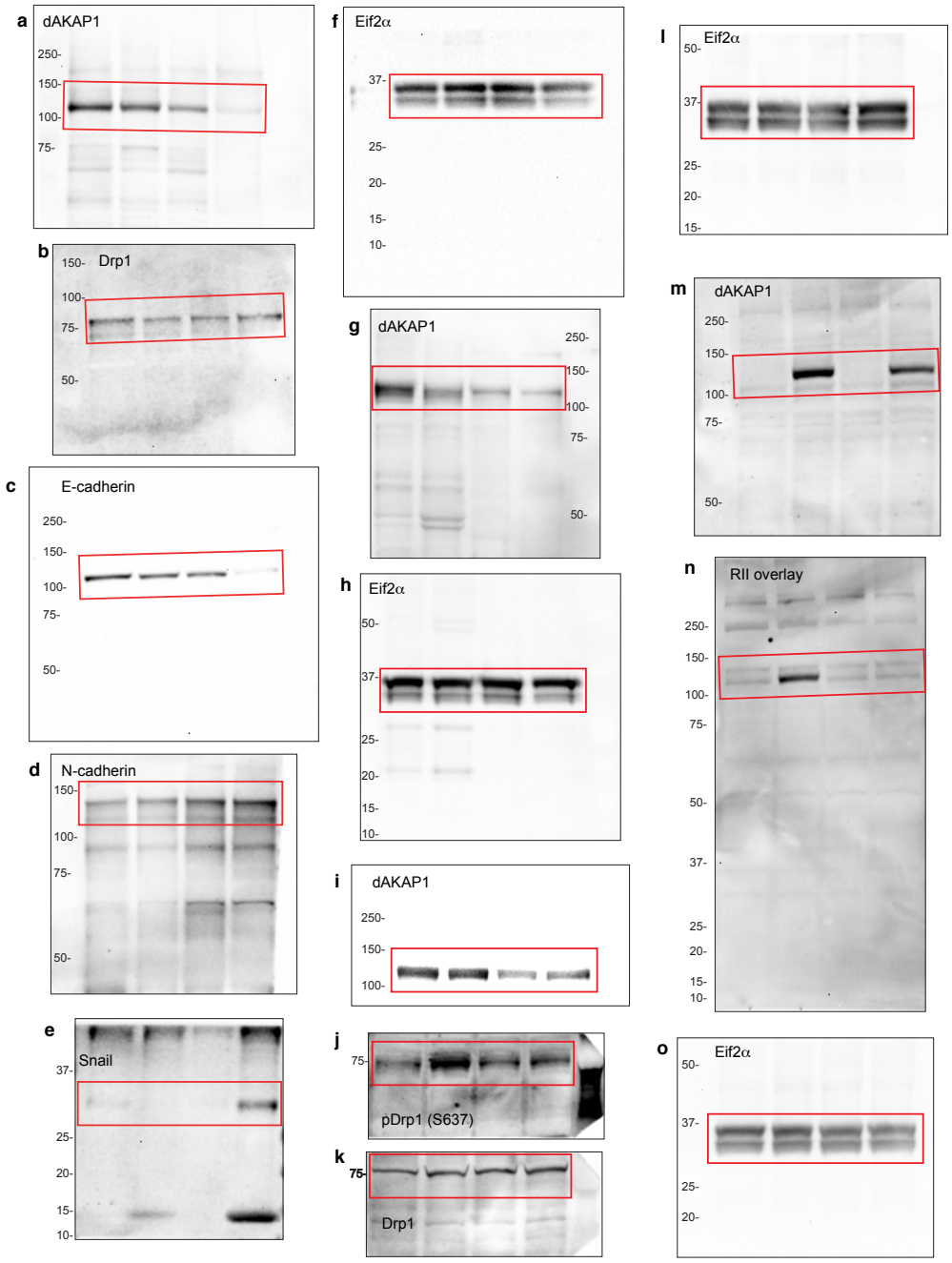

Appendix B. Un-cropped immunoblot images. (a-f) Uncropped immunoblots presented in fig. 2.2c. **(g & h)** Uncropped immunoblots presented in fig. 3.2a. **(i-l)** Uncropped immunoblots presented in fig. 4.2a. **(m-o)** Uncropped blots presented in fig. 5.1a. Primary antibody is indicated in each panel. Molecular weight markers are indicated.

References

1 Surveillance, E., and End Results (SEER) Program (www.seer.cancer.gov). Cancer Statistics Review (1975-2014). (National Cancer Institute, 2017).

2 Kalluri, R. & Weinberg, R. A. The basics of epithelial-mesenchymal transition. *J Clin Invest* **119**, 1420-1428, doi:10.1172/JCI39104 (2009).

3 Thiery, J. P. & Sleeman, J. P. Complex networks orchestrate epithelial-mesenchymal transitions. *Nat Rev Mol Cell Biol* **7**, 131-142, doi:10.1038/nrm1835 (2006).

4 Mani, S. A. *et al.* The epithelial-mesenchymal transition generates cells with properties of stem cells. *Cell* **133**, 704-715, doi:10.1016/j.cell.2008.03.027 (2008).

5 Zeisberg, M. & Neilson, E. G. Biomarkers for epithelial-mesenchymal transitions. *J Clin Invest* **119**, 1429-1437, doi:10.1172/JCI36183 (2009).

6 Gujral, T. S. *et al.* A noncanonical Frizzled2 pathway regulates epithelial-mesenchymal transition and metastasis. *Cell* **159**, 844-856, doi:10.1016/j.cell.2014.10.032 (2014).

7 Vander Heiden, M. G. & DeBerardinis, R. J. Understanding the Intersections between Metabolism and Cancer Biology. *Cell* **168**, 657-669, doi:10.1016/j.cell.2016.12.039 (2017).

8 Sciacovelli, M. & Frezza, C. Metabolic reprogramming and epithelial-to-mesenchymal transition in cancer. *FEBS J* **284**, 3132-3144, doi:10.1111/febs.14090 (2017).

9 Harbeck, N. & Gnant, M. Breast cancer. *Lancet* **389**, 1134-1150, doi:10.1016/S0140-6736(16)31891-8 (2017).

10 Parker, J. S. *et al.* Supervised risk predictor of breast cancer based on intrinsic subtypes. *J Clin Oncol* **27**, 1160-1167, doi:10.1200/JCO.2008.18.1370 (2009).

11 Balduzzi, S. *et al.* Trastuzumab-containing regimens for metastatic breast cancer. *Cochrane Database Syst Rev*, CD006242, doi:10.1002/14651858.CD006242.pub2 (2014).

12 Gold, M. G., Gonen, T. & Scott, J. D. Local cAMP signaling in disease at a glance. *J Cell Sci* **126**, 4537-4543, doi:10.1242/jcs.133751 (2013).

13 Beuschlein, F. *et al.* Constitutive activation of PKA catalytic subunit in adrenal Cushing's syndrome. *N Engl J Med* **370**, 1019-1028, doi:10.1056/NEJMoa1310359 (2014).

14 Canton, D. A. *et al.* Gravin is a transitory effector of polo-like kinase 1 during cell division. *Mol Cell* **48**, 547-559, doi:10.1016/j.molcel.2012.09.002 (2012).

15 Hehnly, H. *et al.* A mitotic kinase scaffold depleted in testicular seminomas impacts spindle orientation in germ line stem cells. *Elife* **4**, e09384, doi:10.7554/eLife.09384 (2015).

16 Kjallquist, U. *et al.* Exome sequencing of primary breast cancers with paired metastatic lesions reveals metastasis-enriched mutations in the A-kinase anchoring protein family (AKAPs). *BMC Cancer* **18**, 174, doi:10.1186/s12885-018-4021-6 (2018).

17 Rinaldi, L. *et al.* Mitochondrial AKAP1 supports mTOR pathway and tumor growth. *Cell Death Dis* **8**, e2842, doi:10.1038/cddis.2017.241 (2017).

18 Langeberg, L. K. & Scott, J. D. Signalling scaffolds and local organization of cellular behaviour. *Nat Rev Mol Cell Biol* **16**, 232-244, doi:10.1038/nrm3966 (2015).

19 Smith, F. D. *et al.* Local protein kinase A action proceeds through intact holoenzymes. *Science* **356**, 1288-1293, doi:10.1126/science.aaj1669 (2017).

20 Herberg, F. W., Maleszka, A., Eide, T., Vossebein, L. & Tasken, K. Analysis of A-kinase anchoring protein (AKAP) interaction with protein kinase A (PKA) regulatory subunits: PKA isoform specificity in AKAP binding. *J Mol Biol* **298**, 329-339, doi:10.1006/jmbi.2000.3662 (2000).

21 Pattabiraman, D. R. *et al.* Activation of PKA leads to mesenchymal-to-epithelial transition and loss of tumor-initiating ability. *Science* **351**, aad3680, doi:10.1126/science.aad3680 (2016).

22 Riggle, K. M. *et al.* Enhanced cAMP-stimulated protein kinase A activity in human fibrolamellar hepatocellular carcinoma. *Pediatr Res* **80**, 110-118, doi:10.1038/pr.2016.36 (2016).

23 Riggle, K. M., Turnham, R., Scott, J. D., Yeung, R. S. & Riehle, K. J. Fibrolamellar Hepatocellular Carcinoma: Mechanistic Distinction From Adult Hepatocellular Carcinoma. *Pediatr Blood Cancer* **63**, 1163-1167, doi:10.1002/pbc.25970 (2016).

24 Cheung, J. *et al.* Structural insights into mis-regulation of protein kinase A in human tumors. *Proc Natl Acad Sci U S A* **112**, 1374-1379, doi:10.1073/pnas.1424206112 (2015).

25 Smith, F. D. *et al.* AKAP-Lbc enhances cyclic AMP control of the ERK1/2 cascade. *Nat Cell Biol* **12**, 1242-1249, doi:10.1038/ncb2130 (2010).

26 Vafai, S. B. & Mootha, V. K. Mitochondrial disorders as windows into an ancient organelle. *Nature* **491**, 374-383, doi:10.1038/nature11707 (2012).

27 Hoppins, S. The regulation of mitochondrial dynamics. *Curr Opin Cell Biol* **29**, 46-52, doi:10.1016/j.ceb.2014.03.005 (2014).

28 Hoppins, S., Lackner, L. & Nunnari, J. The machines that divide and fuse mitochondria. *Annu Rev Biochem* **76**, 751-780, doi:10.1146/annurev.biochem.76.071905.090048 (2007).

29 Eisner, V., Picard, M. & Hajnóczky, G. Mitochondrial dynamics in adaptive and maladaptive cellular stress responses. *Nature Cell Biology* **20**, 755-765, doi:10.1038/s41556-018-0133-0 (2018).

30 DeBerardinis, R. J. & Chandel, N. S. Fundamentals of cancer metabolism. *Sci Adv* **2**, e1600200, doi:10.1126/sciadv.1600200 (2016).

31 Awale, S. *et al.* Identification of arctigenin as an antitumor agent having the ability to eliminate the tolerance of cancer cells to nutrient starvation. *Cancer Res* **66**, 1751-1757, doi:10.1158/0008-5472.CAN-05-3143 (2006).

32 Gomes, L. C., Di Benedetto, G. & Scorrano, L. During autophagy mitochondria elongate, are spared from degradation and sustain cell viability. *Nat Cell Biol* **13**, 589-598, doi:10.1038/ncb2220 (2011).

33 Li, J. *et al.* Mitochondrial elongation-mediated glucose metabolism reprogramming is essential for tumour cell survival during energy stress. *Oncogene* **36**, 4901-4912, doi:10.1038/onc.2017.98 (2017).

34 Chen, H. *et al.* Mitofusins Mfn1 and Mfn2 coordinately regulate mitochondrial fusion and are essential for embryonic development. *J Cell Biol* **160**, 189-200, doi:10.1083/jcb.200211046 (2003).

35 Meeusen, S. *et al.* Mitochondrial inner-membrane fusion and crista maintenance requires the dynamin-related GTPase Mgm1. *Cell* **127**, 383-395, doi:10.1016/j.cell.2006.09.021 (2006).

36 Bleazard, W. *et al.* The dynamin-related GTPase Dnm1 regulates mitochondrial fission in yeast. *Nat Cell Biol* **1**, 298-304, doi:10.1038/13014 (1999).

37 Yoon, Y., Krueger, E. W., Oswald, B. J. & McNiven, M. A. The mitochondrial protein hFis1 regulates mitochondrial fission in mammalian cells through an interaction with the dynamin-like protein DLP1. *Mol Cell Biol* **23**, 5409-5420 (2003).

38 Chen, Y. & Sheng, Z. H. Kinesin-1-syntaphilin coupling mediates activity-dependent regulation of axonal mitochondrial transport. *J Cell Biol* **202**, 351-364, doi:10.1083/jcb.201302040 (2013).

39 Aggarwal-Howarth, S. & Scott, J. D. Pseudoscaffolds and anchoring proteins: the difference is in the details. *Biochem Soc Trans* **45**, 371-379, doi:10.1042/BST20160329 (2017).

40 Chang, C. R. & Blackstone, C. Cyclic AMP-dependent protein kinase phosphorylation of Drp1 regulates its GTPase activity and mitochondrial morphology. *J Biol Chem* **282**, 21583-21587, doi:10.1074/jbc.C700083200 (2007).

41 Cribbs, J. T. & Strack, S. Reversible phosphorylation of Drp1 by cyclic AMP-dependent protein kinase and calcineurin regulates mitochondrial fission and cell death. *EMBO Rep* **8**, 939-944, doi:10.1038/sj.embor.7401062 (2007).

42 Cardone, L. *et al.* Mitochondrial AKAP121 binds and targets protein tyrosine phosphatase D1, a novel positive regulator of src signaling. *Mol Cell Biol* **24**, 4613-4626, doi:10.1128/MCB.24.11.4613-4626.2004 (2004).

43 Acin-Perez, R. *et al.* Cyclic AMP produced inside mitochondria regulates oxidative phosphorylation. *Cell Metab* **9**, 265-276, doi:10.1016/j.cmet.2009.01.012 (2009).

44 Lefkimmiatis, K., Leronni, D. & Hofer, A. M. The inner and outer compartments of mitochondria are sites of distinct cAMP/PKA signaling dynamics. *J Cell Biol* **202**, 453-462, doi:10.1083/jcb.201303159 (2013).

45 Sardanelli, A. M. *et al.* Occurrence of A-kinase anchor protein and associated cAMP-dependent protein kinase in the inner compartment of mammalian mitochondria. *FEBS Lett* **580**, 5690-5696, doi:10.1016/j.febslet.2006.09.020 (2006).

46 Pidoux, G. *et al.* Optic atrophy 1 is an A-kinase anchoring protein on lipid droplets that mediates adrenergic control of lipolysis. *EMBO J* **30**, 4371-4386, doi:10.1038/emboj.2011.365 (2011).

47 Sesaki, H., Southard, S. M., Yaffe, M. P. & Jensen, R. E. Mgm1p, a dynamin-related GTPase, is essential for fusion of the mitochondrial outer membrane. *Mol Biol Cell* **14**, 2342-2356, doi:10.1091/mbc.e02-12-0788 (2003).

48 Wong, E. D. *et al.* The intramitochondrial dynamin-related GTPase, Mgm1p, is a component of a protein complex that mediates mitochondrial fusion. *J Cell Biol* **160**, 303-311, doi:10.1083/jcb.200209015 (2003).

49 Kovanich, D. *et al.* Sphingosine kinase interacting protein is an A-kinase anchoring protein specific for type I cAMP-dependent protein kinase. *Chembiochem* **11**, 963-971, doi:10.1002/cbic.201000058 (2010).

50 Means, C. K. *et al.* An entirely specific type I A-kinase anchoring protein that can sequester two molecules of protein kinase A at mitochondria. *Proc Natl Acad Sci U S A* **108**, E1227-1235, doi:10.1073/pnas.1107182108 (2011).

51 Zhao, J. *et al.* Mitochondrial dynamics regulates migration and invasion of breast cancer cells. *Oncogene* **32**, 4814-4824, doi:10.1038/onc.2012.494 (2013).

52 Xu, K. *et al.* MFN2 suppresses cancer progression through inhibition of mTORC2/Akt signaling. *Sci Rep* **7**, 41718, doi:10.1038/srep41718 (2017).

53 Caino, M. C. *et al.* Syntaphilin controls a mitochondrial rheostat for proliferation-motility decisions in cancer. *J Clin Invest* **127**, 3755-3769, doi:10.1172/JCI93172 (2017).

54 Cunniff, B., McKenzie, A. J., Heintz, N. H. & Howe, A. K. AMPK activity regulates trafficking of mitochondria to the leading edge during cell migration and matrix invasion. *Mol Biol Cell* **27**, 2662-2674, doi:10.1091/mbc.E16-05-0286 (2016).

55 McKenzie, A. J., Campbell, S. L. & Howe, A. K. Protein kinase A activity and anchoring are required for ovarian cancer cell migration and invasion. *PLoS One* **6**, e26552, doi:10.1371/journal.pone.0026552 (2011).

56 Hoffman, N. J. *et al.* Global Phosphoproteomic Analysis of Human Skeletal Muscle Reveals a Network of Exercise-Regulated Kinases and AMPK Substrates. *Cell Metab* **22**, 922-935, doi:10.1016/j.cmet.2015.09.001 (2015).

57 Lin, R. Y., Moss, S. B. & Rubin, C. S. Characterization of S-AKAP84, a novel developmentally regulated A kinase anchor protein of male germ cells. *J Biol Chem* **270**, 27804-27811 (1995).

58 Huang, L. J. *et al.* NH2-Terminal targeting motifs direct dual specificity A-kinase-anchoring protein 1 (D-AKAP1) to either mitochondria or endoplasmic reticulum. *J Cell Biol* **145**, 951-959 (1999).

59 Flippo, K. H. *et al.* AKAP1 protects from cerebral ischemic stroke by inhibiting Drp1-dependent mitochondrial fission. *J Neurosci*, doi:10.1523/JNEUROSCI.0649-18.2018 (2018).

60 Merrill, R. A. *et al.* Mechanism of neuroprotective mitochondrial remodeling by PKA/AKAP1. *PLoS Biol* **9**, e1000612, doi:10.1371/journal.pbio.1000612 (2011).

61 Kim, H. *et al.* Fine-tuning of Drp1/Fis1 availability by AKAP121/Siah2 regulates mitochondrial adaptation to hypoxia. *Mol Cell* **44**, 532-544, doi:10.1016/j.molcel.2011.08.045 (2011).

62 Schiattarella, G. G. *et al.* Akap1 Deficiency Promotes Mitochondrial Aberrations and Exacerbates Cardiac Injury Following Permanent Coronary Ligation via Enhanced Mitophagy and Apoptosis. *PLoS One* **11**, e0154076, doi:10.1371/journal.pone.0154076 (2016).

63 Steen, R. L., Martins, S. B., Tasken, K. & Collas, P. Recruitment of protein phosphatase 1 to the nuclear envelope by A- kinase anchoring protein AKAP149 is a prerequisite for nuclear lamina assembly . *J. Cell Biol.* **150**, 1251-1262 (2000).

64 Asirvatham, A. L. *et al.* A-kinase anchoring proteins interact with phosphodiesterases in T lymphocyte cell lines. *J Immunol* **173**, 4806-4814 (2004).

65 Glaven, J. A., Whitehead, I. P., Nomanbhoy, T., Kay, R. & Cerione, R. A. Lfc and Lsc oncoproteins represent two new guanine nucleotide exchange factors for the Rho GTP-binding protein. *J Biol Chem* **271**, 27374-27381 (1996).

66 Meiri, D. *et al.* Modulation of Rho guanine exchange factor Lfc activity by protein kinase A-mediated phosphorylation. *Mol Cell Biol* **29**, 5963-5973, doi:10.1128/MCB.01268-08 (2009).

67 Barretina, J. *et al.* The Cancer Cell Line Encyclopedia enables predictive modelling of anticancer drug sensitivity. *Nature* **483**, 603-607, doi:10.1038/nature11003 (2012).

68 Hanahan, D. & Weinberg, R. A. Hallmarks of cancer: the next generation. *Cell* **144**, 646-674, doi:10.1016/j.cell.2011.02.013 (2011).

69 Cancer Genome Atlas, N. Comprehensive molecular portraits of human breast tumours. *Nature* **490**, 61-70, doi:10.1038/nature11412 (2012).

70 Mertins, P. *et al.* Proteogenomics connects somatic mutations to signalling in breast cancer. *Nature* **534**, 55-62, doi:10.1038/nature18003 (2016).

71 Chiarugi, P. & Cirri, P. Metabolic exchanges within tumor microenvironment. *Cancer Lett* **380**, 272-280, doi:10.1016/j.canlet.2015.10.027 (2016).

72 Casey, T. *et al.* Molecular signatures suggest a major role for stromal cells in development of invasive breast cancer. *Breast Cancer Res Treat* **114**, 47-62, doi:10.1007/s10549-008-9982-8 (2009).

73 Sotgia, F. *et al.* Mitochondria "fuel" breast cancer metabolism: fifteen markers of mitochondrial biogenesis label epithelial cancer cells, but are excluded from adjacent stromal cells. *Cell Cycle* **11**, 4390-4401, doi:10.4161/cc.22777 (2012).

74 Perrino, C. *et al.* AKAP121 downregulation impairs protective cAMP signals, promotes mitochondrial dysfunction, and increases oxidative stress. *Cardiovasc Res* **88**, 101-110, doi:10.1093/cvr/cvq155 (2010).

75 Neve, R. M. *et al.* A collection of breast cancer cell lines for the study of functionally distinct cancer subtypes. *Cancer Cell* **10**, 515-527, doi:10.1016/j.ccr.2006.10.008 (2006).

76 Pelicano, H. *et al.* Mitochondrial dysfunction in some triple-negative breast cancer cell lines: role of mTOR pathway and therapeutic potential. *Breast Cancer Res* **16**, 434, doi:10.1186/s13058-014-0434-6 (2014).

77 Lawrence, R. T. *et al.* The proteomic landscape of triple-negative breast cancer. *Cell Rep* **11**, 630-644, doi:10.1016/j.celrep.2015.03.050 (2015).

78 Ma, Y. & Taylor, S. S. A molecular switch for targeting between endoplasmic reticulum (ER) and mitochondria: conversion of a mitochondria-targeting element into an ER-targeting signal in DAKAP1. *J Biol Chem* **283**, 11743-11751, doi:10.1074/jbc.M710494200 (2008).

79 Merrill, R. A. & Strack, S. Mitochondria: a kinase anchoring protein 1, a signaling platform for mitochondrial form and function. *Int J Biochem Cell Biol* **48**, 92-96, doi:10.1016/j.biocel.2013.12.012 (2014).

80 Johnson, L. V., Walsh, M. L., Bockus, B. J. & Chen, L. B. Monitoring of relative mitochondrial membrane potential in living cells by fluorescence microscopy. *J Cell Biol* **88**, 526-535 (1981).

81 Livigni, A. *et al.* Mitochondrial AKAP121 links cAMP and src signaling to oxidative metabolism. *Mol Biol Cell* **17**, 263-271, doi:10.1091/mbc.e05-09-0827 (2006).

82 Saris, N. E. & Carafoli, E. A historical review of cellular calcium handling, with emphasis on mitochondria. *Biochemistry (Mosc)* **70**, 187-194 (2005).

83 Jahani-Asl, A. & Slack, R. S. The phosphorylation state of Drp1 determines cell fate. *EMBO Rep* **8**, 912-913, doi:10.1038/sj.embor.7401077 (2007).

84 Liu, X., Weaver, D., Shirihai, O. & Hajnoczky, G. Mitochondrial 'kiss-and-run': interplay between mitochondrial motility and fusion-fission dynamics. *EMBO J* **28**, 3074-3089, doi:10.1038/emboj.2009.255 (2009).

85 Grandemange, S., Herzig, S. & Martinou, J. C. Mitochondrial dynamics and cancer. *Semin Cancer Biol* **19**, 50-56, doi:10.1016/j.semcancer.2008.12.001 (2009).

86 Soubannier, V. & McBride, H. M. Positioning mitochondrial plasticity within cellular signaling cascades. *Biochim Biophys Acta* **1793**, 154-170, doi:10.1016/j.bbamcr.2008.07.008 (2009).

87 Campello, S. *et al.* Orchestration of lymphocyte chemotaxis by mitochondrial dynamics. *J Exp Med* **203**, 2879-2886, doi:10.1084/jem.20061877 (2006).

88 Smirnova, E., Griparic, L., Shurland, D. L. & van der Bliek, A. M. Dynamin-related protein Drp1 is required for mitochondrial division in mammalian cells. *Mol Biol Cell* **12**, 2245-2256, doi:10.1091/mbc.12.8.2245 (2001).

89 Heytler, P. G. & Prichard, W. W. A new class of uncoupling agents--carbonyl cyanide phenylhydrazones. *Biochem Biophys Res Commun* **7**, 272-275 (1962).

90 Mosmann, T. Rapid colorimetric assay for cellular growth and survival: application to proliferation and cytotoxicity assays. *J Immunol Methods* **65**, 55-63 (1983).

91 Quail, D. F. & Joyce, J. A. Microenvironmental regulation of tumor progression and metastasis. *Nat Med* **19**, 1423-1437, doi:10.1038/nm.3394 (2013).

92 McAllister, S. S. & Weinberg, R. A. The tumour-induced systemic environment as a critical regulator of cancer progression and metastasis. *Nat Cell Biol* **16**, 717-727, doi:10.1038/ncb3015 (2014).

93 Smith, F. D. *et al.* Intrinsic disorder within an AKAP-protein kinase A complex guides local substrate phosphorylation. *Elife* **2**, e01319, doi:10.7554/eLife.01319 (2013).

94 Desai, S. P., Bhatia, S. N., Toner, M. & Irimia, D. Mitochondrial localization and the persistent migration of epithelial cancer cells. *Biophys J* **104**, 2077-2088, doi:10.1016/j.bpj.2013.03.025 (2013).

95 Mi, H. *et al.* PANTHER version 11: expanded annotation data from Gene Ontology and Reactome pathways, and data analysis tool enhancements. *Nucleic Acids Res* **45**, D183-D189, doi:10.1093/nar/gkw1138 (2017).

96 Tyanova, S. *et al.* The Perseus computational platform for comprehensive analysis of (prote)omics data. *Nat Methods* **13**, 731-740, doi:10.1038/nmeth.3901 (2016).

97 Dagda, R. K. *et al.* Loss of PINK1 function promotes mitophagy through effects on oxidative stress and mitochondrial fission. *J Biol Chem* **284**, 13843-13855, doi:10.1074/jbc.M808515200 (2009).

98 Jersie-Christensen, R. R., Sultan, A. & Olsen, J. V. Simple and Reproducible Sample Preparation for Single-Shot Phosphoproteomics with High Sensitivity. *Methods Mol Biol* **1355**, 251-260, doi:10.1007/978-1-4939-3049-4_17 (2016).

99 Villen, J. & Gygi, S. P. The SCX/IMAC enrichment approach for global phosphorylation analysis by mass spectrometry. *Nat Protoc* **3**, 1630-1638, doi:10.1038/nprot.2008.150 (2008).

100 Ficarro, S. B. *et al.* Magnetic bead processor for rapid evaluation and optimization of parameters for phosphopeptide enrichment. *Anal Chem* **81**, 4566-4575, doi:10.1021/ac9004452 (2009).

101 Rappsilber, J., Mann, M. & Ishihama, Y. Protocol for micro-purification, enrichment, pre-fractionation and storage of peptides for proteomics using StageTips. *Nat Protoc* **2**, 1896-1906, doi:10.1038/nprot.2007.261 (2007).

102 Golkowski, M. *et al.* Kinobead and Single-Shot LC-MS Profiling Identifies Selective PKD Inhibitors. *J Proteome Res* **16**, 1216-1227, doi:10.1021/acs.jproteome.6b00817 (2017).

103 Cox, J. *et al.* Andromeda: a peptide search engine integrated into the MaxQuant environment. *J Proteome Res* **10**, 1794-1805, doi:10.1021/pr101065j (2011).